U.S. DEPARTMENT OF COMMERCE
National Technical Information Service

PB-262 541

Plume Dispersion in Stably Stratified Flows Over Complex Terrain, Phase 2

Flow Research, Inc, Kent, Wash

Prepared for

Environmental Sciences Research Lab, Research Triangle Park, N C
Meteorology and Assessment Div

May 76

PB 262 541

REPRODUCED BY
NATIONAL TECHNICAL
INFORMATION SERVICE
U.S. DEPARTMENT OF COMMERCE
SPRINGFIELD, VA. 22161

RESEARCH REPORTING SERIES

Research reports of the Office of Research and Development, U.S. Environmental Protection Agency, have been grouped into five series. These five broad categories were established to facilitate further development and application of environmental technology. Elimination of traditional grouping was consciously planned to foster technology transfer and a maximum interface in related fields. The five series are:

1. Environmental Health Effects Research
2. Environmental Protection Technology
3. Ecological Research
4. Environmental Monitoring
5. Socioeconomic Environmental Studies

This report has been assigned to the ENVIRONMENTAL MONITORING series. This series describes research conducted to develop new or improved methods and instrumentation for the identification and quantification of environmental pollutants at the lowest conceivably significant concentrations. It also includes studies to determine the ambient concentrations of pollutants in the environment and/or the variance of pollutants as a function of time or meteorological factors.

This document is available to the public through the National Technical Information Service, Springfield, Virginia 22161.

TECHNICAL REPORT DATA
(Please read Instructions on the reverse before completing)

1. REPORT NO. EPA-600/4-76-022	2.
3. RECIPIENT'S ACCESSION NO.	
4. TITLE AND SUBTITLE PLUME DISPERSION IN STABLY STRATIFIED FLOWS OVER COMPLEX TERRAIN Phase 2	5. REPORT DATE May 1976 6. PERFORMING ORGANIZATION CODE
7. AUTHOR(S) H. T. Liu and J. T. Lin	8. PERFORMING ORGANIZATION REPORT NO. Flow Research Report No. 57
9. PERFORMING ORGANIZATION NAME AND ADDRESS Flow Research, Inc. 1819 South Central Avenue Kent, Washington 98031	10. PROGRAM ELEMENT NO. 1AA009 11. CONTRACT/GRANT NO. 68-02-1293
12. SPONSORING AGENCY NAME AND ADDRESS Environmental Sciences Research Laboratory Office of Research and Development U. S. Environmental Protection Agency Research Triangle Park, NC 27711	13. TYPE OF REPORT AND PERIOD COVERED Final Report, 5/74-3/75 14. SPONSORING AGENCY CODE EPA - ORD
15. SUPPLEMENTARY NOTES	

16. ABSTRACT

Laboratory experiments were conducted in a stratified towing tank to investigate plume dispersion in stably stratified flows. First, plume dispersion over an idealized terrain model with a simulated elevated inversion in the atmosphere was investigated. These results were compared with those of experiments previously conducted under simulated ground inversions. Second, plume dispersion in 1-layer stably stratified flows over a realistic terrain was also modeled. The plume dispersion patterns showed a strong interaction between the stratified flow and the rugged terrain features. Third, plume dispersion during inversion breakup was simulated. Results indicated that as soon as the convective layer built to reach the plume, pollutants were stirred and carried to the ground.

17. KEY WORDS AND DOCUMENT ANALYSIS

a. DESCRIPTORS	b. IDENTIFIERS/OPEN ENDED TERMS	c. COSATI Field/Group
*Tests		14B
*Plumes		21B
*Atmospheric diffusion		04A
*Stratification		14G
*Terrain		08F
Air pollution		13B

18. DISTRIBUTION STATEMENT RELEASE TO PUBLIC	19. SECURITY CLASS (This Report) UNCLASSIFIED	21. NO. OF PAGES 68
	20. SECURITY CLASS (This page) UNCLASSIFIED	22. PRICE $4.50

EPA Form 2220-1 (9-73)

EPA-600/4-76-022
May 1976

PLUME DISPERSION IN STABLY STRATIFIED FLOWS OVER COMPLEX TERRAIN
Phase 2

by

H. T. Liu and J. T. Lin
Flow Research, Inc.
Kent, Washington 98031

Contract No. 68-02-1293

Project Officer

William H. Snyder
Meteorology and Assessment Division
Environmental Sciences Research Laboratory
Research Triangle Park, N.C. 27711

ENVIRONMENTAL SCIENCES RESEARCH LABORATORY
OFFICE OF RESEARCH AND DEVELOPMENT
U. S. ENVIRONMENTAL PROTECTION AGENCY
RESEARCH TRIANGLE PARK, N.C. 27711

DISCLAIMER

This report has been reviewed by the Environmental Sciences Research Laboratory, U. S. Environmental Protection Agency, and approved for publication. Approval does not signify that the contents necessarily reflect the views and policies of the U. S. Environmental Protection Agency, nor does mention of trade names of commercial products constitute endorsement or recommendation for use.

PREFACE

Flow Research has been under contract with the Environmental Protection Agency (Contract No. 68-02-1293) to continue investigation of plume dispersion in stably stratified flows over complex terrain. Two tasks are involved:

Task I - Laboratory simulation of plume dispersion in stably stratified flows over complex terrain.

Task II - Development of a numerical model using a small-Froude-number asymptotic expansion to simulate strongly stratified flows over complex terrain.

The final report consists of two task-oriented parts, each of which is an individual report. The first is entitled "Plume Dispersion in Stably Stratified Flows Over Complex Terrain: Phase 2," and the second is entitled "A Numerical and Experimental Study of Stably Stratified Flow Around Complex Terrain." In addition, a 16mm color film entitled "Laboratory Simulation of Stratified Flows Over Complex Terrain," in which most of the visualization results for both tasks are summarized, is included as an essential supplement to this final report.

ABSTRACT

Laboratory experiments were conducted in a stratified towing tank to investigate plume dispersion in stably stratified flows. First, plume dispersion over an idealized terrain model with simulated elevated inversions was investigated. These results were compared with those of experiments previously conducted for simulated ground inversions. Second, plume dispersion in 1-layer stably stratified flows over a realistic terrain was modeled. The plume dispersion patterns showed a strong interaction between the stratified flow and the rugged terrain features. The third experiment was a simulation of plume dispersion during inversion breakup. Results indicated that pollutants were stirred and carried to the ground as soon as the convective layer reached the plume that was originally trapped in the inversion layer.

CONTENTS

Preface iii
Abstract iv
List of Figures vi
List of Tables viii
List of Symbols ix

I. Introduction 1
II. Summary 4
III. Conclusions 5
IV. Laboratory Facilities 8
V. Plume Dispersion in 3-Layer Stratified Flows 19
VI. Plume Dispersion From the Kennecott Smelter Stack 29
VII. Plume Dispersion During Inversion Breakup 36

References 46
Appendices

A. The Effect of an Absorptive Layer on Plume Dispersion . . 48
B. The Effect of an Exaggerated Stack on Plume Dispersion . 51
C. The Response of a Hot-Film Probe to a Variation of Fluid Density 53

LIST OF FIGURES

Number		Page
1	A Contour Map of the Idealized Terrain Model	10
2	Terrain Model in the Vicinity of the Kennecott Copper Smelter in Garfield, Utah	12
3	A Block Diagram of the Effluent Injection Device	14
4	Calibration Curves of a Thermistor Probe	16
5	A Typical 3-Layer Stratification Profile Measured With a Conductivity Probe in the Towing Tank (Runs IIa and IIb) . .	18
6	3-Layer Stratification Structure for the Simulation of Plume Dispersion Into an Elevated Inversion Layer	20
7	Plume Dispersion Into an Elevated Inversion Layer Over the Idealized Terrain Model. $F_D = 3.08$	21
8	Mean Velocity Profile at the Location of the Stack in Run IIb. The Ambient Fluid Was Stratified with a 3-Layer Structure. The Idealized Terrain Model Was That Described in Section 5.9	25
9	Dye Visualization of Plume Dispersion From a Stack Located at the Kennecott Copper Smelter in Garfield, Utah, Under Stable Conditions. Wind Direction = 315°. $F_D = 2.02$ . . .	31
10	Mean Velocity Profiles at the Location of the Stack in the Kennecott Smelter Model. Wind Direction = 315°	34
11	Typical and Idealized Temperature Profiles for the Inversion Breakup Experiment (see Thomas, et al., 1970)	40
12	Penetration Height $z_i(t)$ of an Unstable Layer Generated by Cooling a Surface With Dry Ice in a Stratified Fluid ($N \sim .1$ Hz)	41
13	Shadowgraph Pictures of Entrainment of Pollutants in a Growing Unstable Layer During Inversion Breakup. $U_\infty = 0$, $N = .09$ Hz, $K = \infty$, $F_H = 0$, $F_D = 3.15$	42
14	Dye Visualization of the Sequential Entrainment of Pollutants (Fumigation) in a Growing Unstable Layer During Inversion Breakup. The Pictures Were Taken With the Camera Stationary to the Towing Tank (Following the Same "Patch" of the Plume)	44

LIST OF FIGURES (CON'T)

Number		Page
15	Temperature Profiles During the Growth of an Unstable Layer Adjacent to a Surface in a Stratified Fluid (N = .095 Hz). The Growth of the Unstable Layer Was Generated by Cooling the Surface With Dry Ice	45
16	Dye Visualization of Plume Dispersion in a Stratified Flow Over the Idealized Terrain Model. An Absorptive Layer Was Installed To Reduce Internal-Wave Reflection. F_D = 3.11. See Figs. 17 and 18 in [I] for Comparison	50

LIST OF TABLES

Number		Page
1	Summary of Experiments	2
2	Simulation Conditions for the Sharp Inversion Experiments	11
3	Ground Concentrations Data of the Sharp Inversion Experiments	27
4	Simulation Conditions for Plume Dispersion From the Kennecott Copper Smelter Stack	30
5	Simulation Conditions for the Inversion Breakup Experiments	38

LIST OF SYMBOLS

SYMBOL	DESCRIPTION	DIMENSION*
B	a buoyancy number defined in eq. (B.1)	-
$\overline{C}$	mean pollutant concentration	$ML^{-2}T^{-2}$
$\overline{C}_a$	ambient pollutant concentration	$ML^{-2}T^{-2}$
$\overline{C}_s$	source pollutant concentration	$ML^{-2}T^{-2}$
D	stack diameter	L
F	buoyancy flux of a plume	L^4T^{-3}
F_D	stack Froude number, $\dfrac{W_s}{\sqrt{\frac{\Delta\rho}{\rho_s} gD}}$	-
F_H	internal Froude number based on the stack height, $\dfrac{U_\infty}{NH}$	-
F_h	internal Froude number based on h, $\dfrac{U}{Nh}$	-
F_{hi}	internal Froude number based on the Brunt-Vaisala frequency at the i^{th} layer, $\dfrac{U}{N_i h}$	-
g	gravitational acceleration	LT^{-2}
H	stack height	L
h	characteristic height, such as that of a mountain	L
K	ratio of effluent velocity to free-stream velocity, $\dfrac{W_s}{U_\infty}$	-
L_D	exaggeration factor of the stack diameter	-
N	Brunt-Vaisala frequency, $\dfrac{1}{2\pi}\sqrt{\dfrac{g}{\rho_a}\dfrac{d\overline{\rho}}{dz}}$	T^{-1}
R_D	stack Reynolds number, $\dfrac{W_s D}{\nu}$	-
R_h	Reynolds number based on the ridge height, $\dfrac{U_\infty h}{\nu}$	-
s	a stability parameter, $(2\pi N)^2$	T^{-2}
T	a time scale defined as the ratio of the length scale to the velocity scale	T

*L = length, T = time, τ = temperature, M = mass

LIST OF SYMBOLS

SYMBOL	DESCRIPTION	DIMENSION*
T_i	time required for the unstable layer to reach its maximum height	T
t	time	T
$\overline{U}(z)$	mean velocity component in x direction	LT^{-1}
U_∞	free-stream velocity	LT^{-1}
w	vertical velocity component	LT^{-1}
w_*	a convective velocity scale	LT^{-1}
W_s	stack effluent velocity	LT^{-1}
x.y.z	Cartesian coordinate axes in longitudinal, lateral and vertical directions, respectively	L
Z	plume trajectory above the stack exit	L
Z_b	elevation of a lower boundary in the towing tank	L
Z_t	final height of the top of a plume in a calm environment	L
Z_u	elevation of an upper boundary in the atmosphere	L
z_i	the height of the penetrative layer	L
$\Delta\rho$	density difference, $\lvert\rho_s - \rho_a\rvert$	ML^{-3}
θ	fluctuating temperature	τ
$\overline{\theta}$	mean temperature	τ
$\overline{\theta}_s$	mean effluent temperature	τ
ρ_a	density of the ambient fluid at stack exit level	ML^{-3}
ρ_s	stack effluent density	ML^{-3}

*L = length, T = time, τ = temperature, M = mass

SECTION I

INTRODUCTION

The objective of this study is to investigate plume dispersion over complex terrain in stably stratified flows under several conditions which might lead to serious pollution episodes. This study is a continuation of the laboratory investigation of plume dispersion over an idealized terrain in a 1-layer stratified flow, which simulates a ground inversion (Lin, et al., 1974 - hereafter referred to as [I]). References to [I] are made frequently to ensure continuity, to provide cross-examination and to minimize unnecessary duplication.

The present study consists of three (3) subtasks, which are summarized in table 1. A brief description of each subtask is given in the following.

The first subtask is the investigation of the plume dispersion over an idealized terrain model (used in [I]) in a 3-layer stratified flow. The three layers consisted of a neutral layer next to the ground, a neutral or a stable layer far above the ground, and an extremely stable layer or inversion layer in between. We then compare the results with those obtained in [I] in a 1-layer stratified flow.

Under the second subtask, we conducted experiments of plume dispersion over a realistic terrain model in a 1-layer stable flow. The realistic terrain chosen was the Kennecott Copper Smelter vicinity including part of Great Salt Lake and part of Oquirrh Mountain. The terrain features are highly rugged and asymmetric, compared to those of the idealized terrain. We selected one of the existing smelter stacks as the pollutant source in the experiment. Results are compared with those obtained by Veenhuizen, et al. (1973), who modeled the same terrain under neutral conditions.

The third subtask is the development of a method which simulates plume dispersion during inversion breakup. Pollutants once aloft and trapped in the inversion layer are subsequently mixed and brought to the ground by the convective motion which develops in the growing unstable layer adjacent to the ground. Using either mass or heat released from a surface into a stratified fluid, we conducted several tests in an attempt to simulate the growth of the unstable layer, and we concluded that heat release provided a more natural and realistic simulation than mass release.

Table 1. Summary of Experiments

a. Plume Dispersion Experiments

Run Number	Description	Terrain Model	Stratification Profile	K	F_h	F_D
Ia	Simulation of Plume Dispersion into an Elevated Inversion	Idealized Terrain Model (eq. 3.1)	3-layer (N-S-N)*	6.8	∞, .92, ∞	3.08
Ib	Simulation of Plume Dispersion into an Elevated Inversion	Idealized Terrain Model (eq. 3.1)	3-layer (N-S-N)	3.4	∞, 1.85, ∞	3.08
IIa	Simulation of Plume Dispersion into an Elevated Inversion	Idealized Terrain Model (eq. 3.1)	3-layer (N-S-S)	6.8	∞, .68, 1.54	3.07
IIb	Simulation of Plume Dispersion into an Elevated Inversion	Idealized Terrain Model (eq. 3.1)	3-layer (N-S-S)	3.4	∞, 1.37, 3.08	3.07
IIIa	Simulation of Plume Dispersion in Stably Stratified Flows Over Complex Terrain	Kennecott Copper Smelter (figs. 2 and 9)	1-layer (S)	2.0	1.04	2.02
IIIb	Simulation of Plume Dispersion in Stably Stratified Flows Over Complex Terrain	Kennecott Copper Smelter (figs. 2 and 9)	1-layer (S)	1.0	2.08	2.02

b. Inversion Breakup

	Description	Terrain Model	Stratification Profile	K	F_h	F_D
-	Simulation of Plume Dispersion During Inversion Breakup (Prototype Condition-TVA Paradise Plant 9-13-1966)	Flat Surface	1-layer (S)	∞, 3.76	∞, 6.10**	3.15

* N = neutral, S = stable

** Based on the stack height

Section III summarizes the important findings of this investigation. Section IV of this report describes the laboratory facility. Sections V, VI and VII present, respectively, the results of the three subtasks described above. The visualization results are also presented in a 16mm color film entitled "Stably Stratified Flows Over Complex Terrain."

SECTION II

SUMMARY

Laboratory experiments in a stratified towing tank were conducted to investigate plume dispersion over a complex terrain for various inversion conditions. The existence of strong vertical shear with alternating overshooting and blocked regions characterized the flow field.

For plume dispersion over an idealized terrain model with simulated elevated inversions, pronounced impingement of pollutants onto the mountain slopes was observed. In this case, more pollutants were carried around the model than in previous experiments conducted under weaker ground inversions.

When the idealized model was replaced by a realistic model in a 1-layer stably stratified flow, which was highly rugged and asymmetric, the dispersion pattern of the latter showed a strong interaction between the stratified flow and the rugged terrain features. The plume axis of the latter showed a lateral diversion of 20° from the free-stream wind direction because of upstream blocking.

Lastly, the feasibility of simulating plume dispersion inversion breakup was successfully demonstrated by cooling a simulated ground surface. Pollutants were stirred and carried to the ground as soon as the convective layer reached the plume originally trapped in the inversion layer.

SECTION III

CONCLUSIONS

3.1 Plume Dispersion in 3-Layer Stratified Flows

(i) The bent-over plumes level off and are trapped within the middle inversion layer. Upstream of the mountain, the vertical spread of the plume is larger than that in a 1-layer stable flow as a result of the relatively large spreading rate in the bottom neutral layer.

(ii) For all the cases, the wind carries the pollutants in the plume at least partially around the mountain. For the cases with a more stable middle-inversion layer, most pollutants are carried around the mountain.

(iii) Direct impingement of pollutants on the mountain slopes is evident from both visualization results and probe measurements. For the cases with a less stable middle layer and a neutral upper layer, the measurement made on the mountain ridge along the center line of the model has the maximum concentration. For the cases with a more stable middle layer, ground concentrations on the ridge are low because most pollutants are carried around the mountain.

(iv) For the low internal-Froude-number, F_{h2}, cases, the pollutants remain aloft both upstream and downstream of the mountain. The vertical spreads are small. For the high internal-Froude-number cases, the wind forces pollutants downward as it carries them around the mountain. Downstream of the mountain, pollutants appear to be stirred and carried to the ground.

(v) Downslope wind is not as strong as that in a linearly stratified case because the lee wave cannot penetrate into the bottom neutral layer.

(vi) At the stack location, the velocity profile (Run IIb), $\overline{U}(z)$, shows a minimum wind-speed region in the middle inversion layer, where the flow is blocked by the mountain ridge. Pronounced shear regions are present in the regions near the interfaces of layers. Strong overshooting occurs in the upper layer.

3.2 Plume Dispersion From the Kennecott Smelter Stack

(i) Under the simulated conditions, the plumes for both cases (F_h = 1.04 and 2.08) are quite close to the ground. The vertical and lateral spreads, especially far downstream of the stack, increases with the internal Froude number.

(ii) For the low internal-Froude-number case (F_h = 1.04), the plume is aloft throughout the entire length of the model. The overall plume shape conforms closely with the underlying terrain features. When the internal Froude number increases (F_h = 2.08), the thickness of the turbulent boundary layer (TBL) increases to include the plume. As a result, pollutants are stirred and carried to the ground. For both cases, however, the ground concentrations are low.

(iii) The wind carries the plumes around Oquirrh Mountain. The plume was trapped within Little Valley. We observe a 20° initial diversion for both cases. For the high internal-Froude-number case, the wind forces the plume slightly farther away from the foothill of Oquirrh Mountain.

(iv) Velocity profiles show that large overshooting occurs at a level high above the terrain surface and is a result of the blocking by the tall and massive mountain ridge. The plumes level off and remain in the blocked region.

3.3 Plume Dispersion During Inversion Breakup

(i) Simulation of inversion breakups have been successfully performed by cooling a model surface using dry ice as the coolant. The shadowgraph records have shown many interesting features, such as the developments of the growing domes, the receding cusps, the sharp interface, etc., which actually occur in the atmosphere.

(ii) Both the penetration height and the duration of occurrence have been realistically scaled. The initial penetration height increases with $t^{1/2}$, in agreement with other data.

(iii) From the visualization results, we have clearly demonstrated the capability of simulating the sequential occurrence of the entrainment of pollutants into the unstable layer.

SECTION IV

LABORATORY FACILITIES

4.1 The Stratified Towing Tank

All experiments, except those concerning inversion breakup, were conducted in a stratified towing tank, 18.3 m long, 1.2 m wide and .9 m deep. A detailed description of this facility appears in a previous FRI report (Pao, et al., 1971). Several features of the towing tank system which are pertinent to the present investigation are described briefly in the following: (i) It has a specially-designed filling system, which facilitates the preparation of a stratified fluid having a predetermined density profile. (ii) It has transparent side and bottom walls, which allow visualization experiments from several directions. (iii) It has a smooth, oil-lubricated carriage, which has a noise level that is approximately 0.3% of the towing speed. The low noise level permits accurate measurements of the velocity, temperature and salinity fluctuations with hot-film probes, thin-film and/or thermistor probes, and single-electrode conductivity probes. (iv) It has a minicomputer system for direct, on-line, multiple-channel, data acquisition and subsequent, statistical, data analysis.

In addition, we installed an absorptive layer made of 7-layer nylon netting on the bottom of the towing tank to reduce internal wave reflection. The nylon netting is knitted with .12-cm braided threads and has diamond-shaped openings (1.3 cm x 1.3 cm). The distance between layers was approximately .6 to 1.2 cm. As an internal wave travels through the absorptive layer, we observed, from shadowgraph pictures, turbulence generated in the wakes of the nylon threads. The generation of turbulence, which is finally damped by the stable stratification, dissipates the energy of the internal wave. To compare the overall dispersion patterns of two plumes released in a stable flow, with and without the absorptive layer in place, we conducted several experiments. The results showed no significant difference between the corresponding cases (see appendix A).

The inversion breakup experiment took place in a stratified towing tank, which was 7.3 m long, .20 m wide, and .71 m deep. This towing tank has the same special features as the larger one, except the tracks of the smaller tank are not oil lubricated.

4.2 Terrain Models

During the experiment, we mounted the terrain models and the stack upside down on an oil-lubricated carriage in the stratified towing tank. To simulate a buoyant plume in the atmosphere, we injected a heavy plume from the inverted stack into the ambient fluid. The plume was traced with dye, and 35mm still-picture cameras and 16mm movie cameras recorded the dispersion patterns. We presented the flow visualization results in such a way that the plume appeared to be injected upward, as in the prototype.

In the sharp inversion experiments (Run Ia, Ib, IIa and IIb), we used the idealized model described in [I]. Figure 1 shows a contour map of the model. The characteristic lengths of the model and the stack are summarized in table 2.

The vicinity of the Kennecott Copper Smelter in Garfield, Utah was modeled for the experiments of plume dispersion over realistic terrain under stable conditions. Figure 2 is a topographic map of the area in the vicinity of the smelter. The stack under investigation is located about 1 km west of Smelter Peak. The surrounding terrain features are extremely rugged. The terrain model, with a scale of 1/10,000 was designed to include terrain features for a far-field simulation of the stack plume. The model covered an area roughly 11 km wide and 30 km long (extending 10 km into Salt Lake in the north and northwest directions, and 11 km in the south and southeast directions). The modeled area includes Kessler Peak (elev. 2689 m) and Coon or Farnsworth Peak (elev. 2760 m) of Oquirrh Mountain. We chose the characteristic height h for the internal Froude number to be the difference between the elevations of Coon Peak and Salt Lake (elev. 1280 m). The model was 1.1 m wide and 3 m long and simulated a wind direction of 315°. The model surfaces were intentionally stepped with vertical steps of .31 cm, corresponding to 30.5-m contour intervals in the prototype.

4.3 The Effluent Injection Device

The effluent was a concentrated dye solution (brilliant-blue food dye) with a predetermined density. The injection device consisted of a heated flask containing the effluent fluid, a temperature controller (YSI Model 72), a veristaltic pump (Monostat Model 72-895-05) with insulated Tygon tubing,

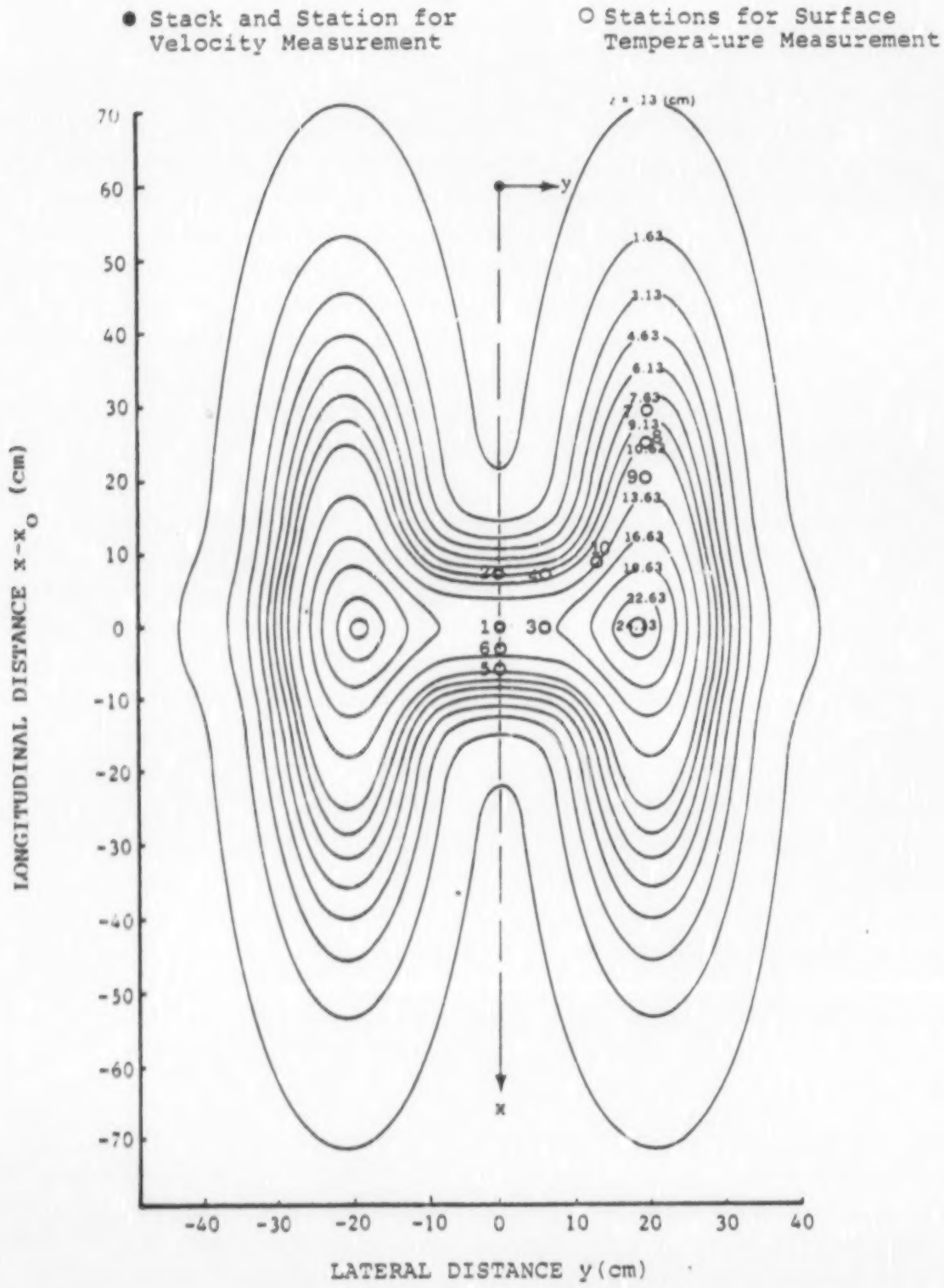

Fig. 1 A Contour Map of the Idealized Terrain Model

Table 2. Simulation Conditions for the Sharp Inversion Experiments

a. Characteristic Length of the Idealized Terrain Model

Length Scale: 1/2,500

Descriptions	Prototype [m]	Model [cm]
Stack Diameter, D	7.94	.32
Stack Height, H	127.0	5.08
Mountain Peaks Height, h_o	609.6	24.38
Mountain Peaks Separation	941.0	37.64
Mountain Ridge Height, h	406.4	16.26

b. Simulation Conditions

Velocity Scale: 1/100

Run Number	U_∞ [cm/s]	K	F_D	Layer	Top of Layer [cm]	N [Hz]	F_h	$\frac{-\partial\bar{\theta}}{\partial z}$ [°C/100m] (prototype)
Ia	3	6.8	3.08	1	9.7	0	∞	-.98
				2	17.8	.20	.92	6.23
				3	40.6	0	∞	-.98
Ib	6	3.4	3.08	1	9.7	0	∞	-.98
				2	17.8	.20	1.85	6.23
				3	40.6	0	∞	-.98
IIa	3	6.8	3.07	1	8.6	0	∞	-.98
				2	19.3	.27	.68	12.22
				3	55.9	.12	1.54	1.59
IIb	6	3.4	3.07	1	8.6	0	∞	-.98
				2	19.3	.27	1.37	12.22
				3	55.9	.12	3.08	1.59

$\rho_s = 1.175$ [gm/cm^3]

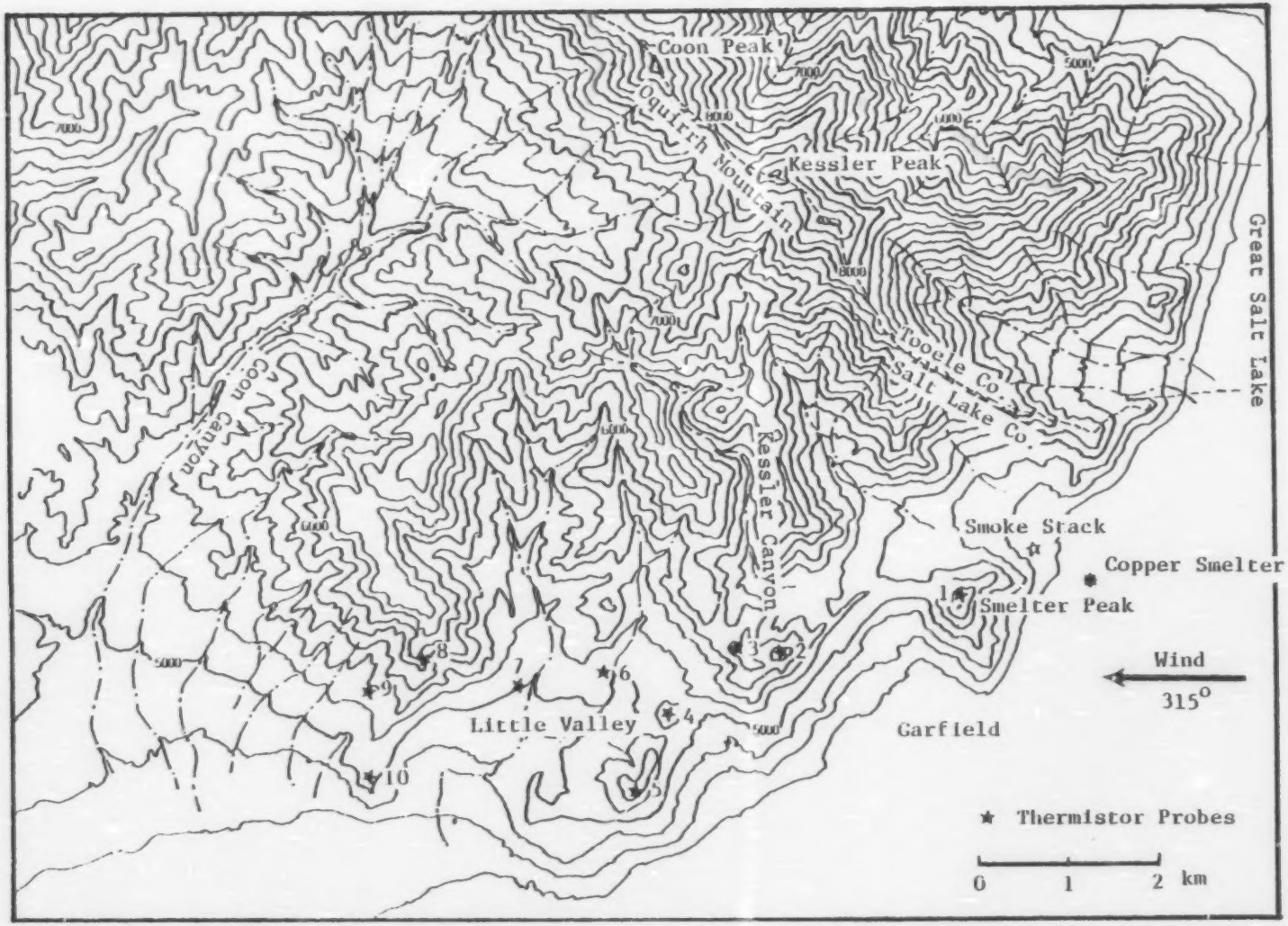

Fig. 2 Terrain Model in the Vicinity of the Kennecott Copper Smelter in Garfield, Utah.

an accumulator, and a heated hose (Technical Heaters, Inc., Model 352) connected to the stack. Figure 3 is a block diagram of the device. After preheating the dye solution to 80°C in the flask, we pumped it through the stack into the ambient fluid and, just upstream of the stack, reheated the effluent in the heated hose, which maintained the temperature at 90 ± 2°C. Fine temperature control was essential since thermistor probes measured the temperature at the terrain surface downstream of the stack to indicate ground concentration. Prior to each experiment, we calibrated the effluent discharge rate with a stopwatch and a graduated cylinder.

To ensure a turbulent plume at the stack exit, we installed a sapphire nozzle ranging from .13 mm to .38 mm in diameter about .5 cm upstream of the stack exit. The size of the nozzle is dependent upon the flow rate and the stack diameter. As the effluent passed through the nozzle, it expanded to the designed size at the stack exit. At a constant discharge rate, the stack Reynolds number is inversely proportional to the nozzle diameter.

4.4 Instrumentation

Two, 10-channel, constant-temperature anemometers (Models 1051-10 and 1053-B, Thermo Systems, Inc.) using fourteen (14) conical and cylindrical hot-film sensors (TSI Models 1230S and 1290 AK) measured the mean and fluctuating velocities of the approaching flow near the stack. The sensors were insulated with two coats of quartz for use in conductive fluid. The system has a frequency response of up to 1 kHz. Hot-film sensors mounted on a strut measured the vertical velocity profiles. These sensors covered a vertical distance of 30 cm, and the spacing decreased between sensors toward the terrain surface. We calibrated the sensors either before or after each velocity measurement with the strut lowered to a distance (the model was upside down) at which no sensors were within the turbulent boundary of the terrain model. For the extreme cases (Runs IIa and IIb), the maximum specific gravity change was about .03 and the corresponding corrections required for the sensor were -8% and +6% for the mean and fluctuating measurements, respectively (appendix C). Five towing speeds were used for the calibration, and the data points were least-squares fitted with second-degree polynominals.

The plumes used in the study were basically turbulent although they tended to relaminarize far downstream of the stack under extremely stable

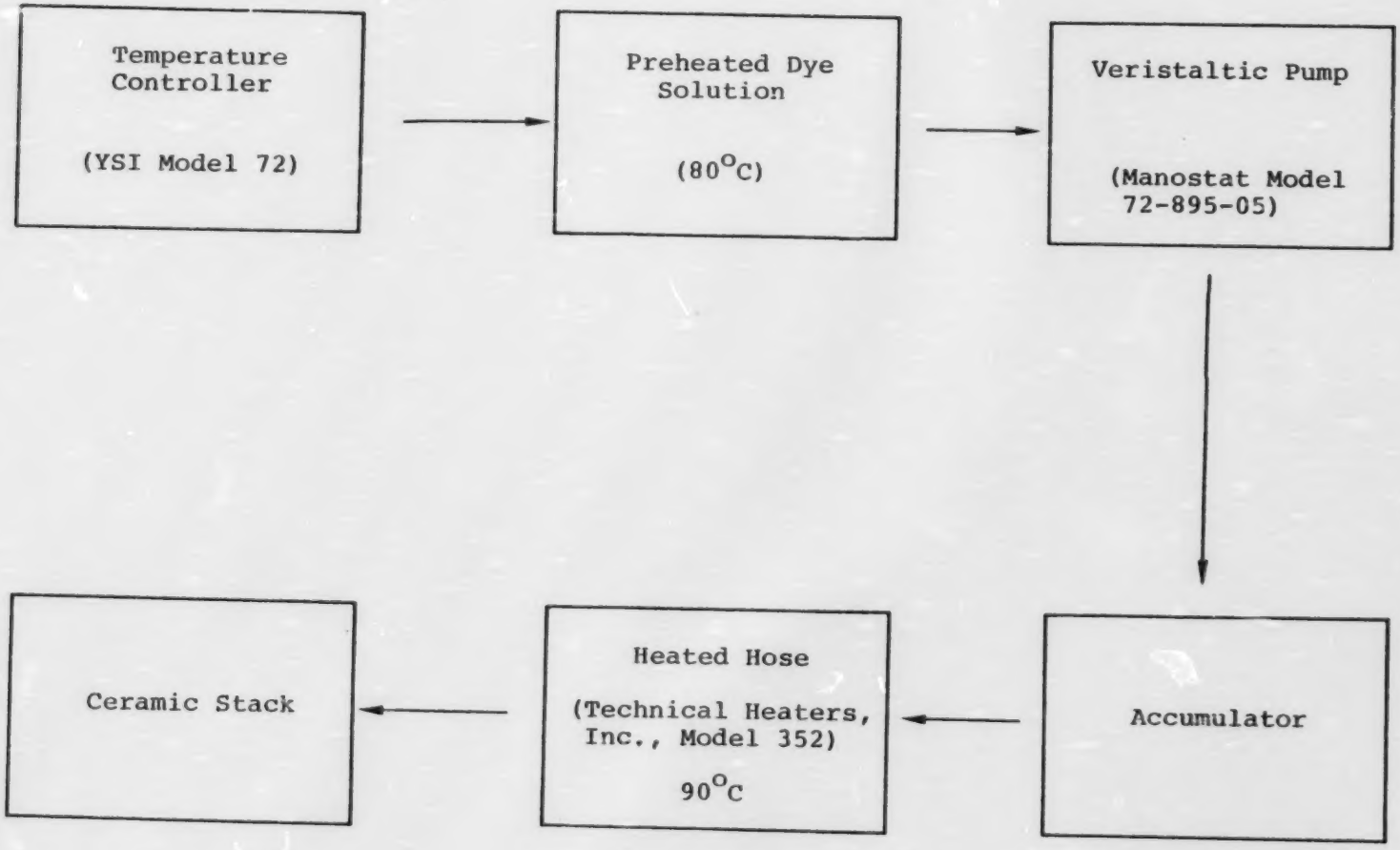

Fig. 3 A Block Diagram of the Effluent Injection Device

conditions. In a turbulent flow, the ratio of the turbulent diffusivity of salinity to that of heat is approximately unity. Therefore, the temperature concentration measured in the model can be directly extrapolated to the field (see eq. (4.1)). Using the temperature as a tracer, we measured ground concentrations with the thermistor probes (Fenwal Electronics GC32SM2). The thermistor probes have a nominal resistance of 2000 Ω and a temperature coefficient of -3.4%/°C at room temperature. The probe tip is 0.76 mm in diameter, and the time constant (3db point) of the thermistor probes in still water is about .07 sec. A 10-channel gauge with the thermistor probe as one arm of the wheatstone bridge measured the temperature of the fluid. The sensitivity of the system is typically 10 volt/°C. The output of the gauge went directly into the minicomputer system for on-line calibration and data acquisition. Signal conditioners increase the overall sensitivity of the temperature gauge to 30 volt/°C with a noise level equivalent to 1.4×10^{-4} °C, and the thermistor probe has long-term stability (a typical drift of .01°C/year). The probes are pre-calibrated against a precision thermometer with .01°C divisions (Brooklyn Thermometer Company, Inc.) in a constant-temperature bath, which is equipped with a temperature controller (YSI Model 72) of .01°C repeatability. In the range of temperature differences of interest (0 ~ .5°C), the calibration curves appear to be quite linear. We used second-degree polynominals to best fit the calibration data. Before each experiment, we measured a reference temperature in the towing tank and fed it into the computer. The computer shifted the recorded calibration curve so that is was parallel to the pre-calibrated curve. Figure 4 is two typical calibration curves of the thermistor probes. For ground concentration measurements, we installed the probes in the terrain model with the probe tips exposed to the ambient fluid at a distance approximately .2 cm above the terrain surface. We then measured and recorded the coordinates of the probes, in reference to the stack. When extrapolated to the field, the following analogy can be made

$$\left[\frac{\overline{\theta} - \overline{\theta}_a}{\overline{\theta}_s - \overline{\theta}_a}\right]_m = \left[\frac{\overline{C} - \overline{C}_a}{\overline{C}_s - \overline{C}_a}\right]_p \qquad (4.1)$$

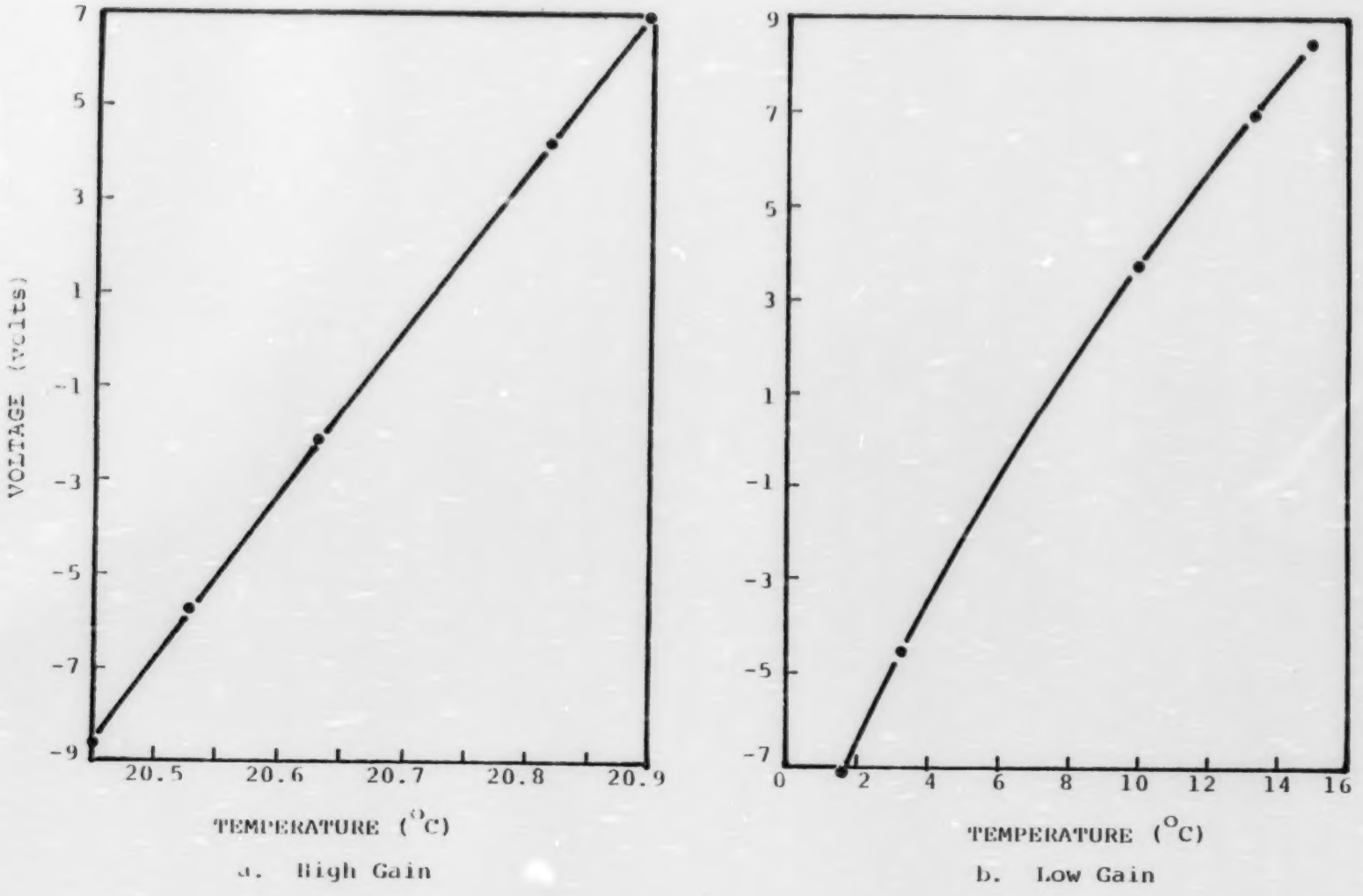

Fig. 4 Calibration Curves of a Thermistor Probe

where $\overline{C}$ is the mean pollutant concentration, $\overline{C}_a$ is the ambient concentration and $\overline{C}_s$ is the source concentration.

A conductivity gauge (Model 1110) developed by Flow Research, Inc., measured the density profiles in the tank. This gauge has a frequency response of from DC to 1 kHz. The sensor was a single-electrode conductivity probe, which has a .025-mm stainless-steel tip platinized with platinum black solution. The sensitivity of the conductivity gauge is about 1 volt per 0.025 gm/cm^3. The probe was calibrated in jars of salt solution of known density, and the calibration data were least-squares fitted with a second-degree polynominal. Figure 5 shows a 3-layer stratification profile measured with a conductivity probe in the towing tank.

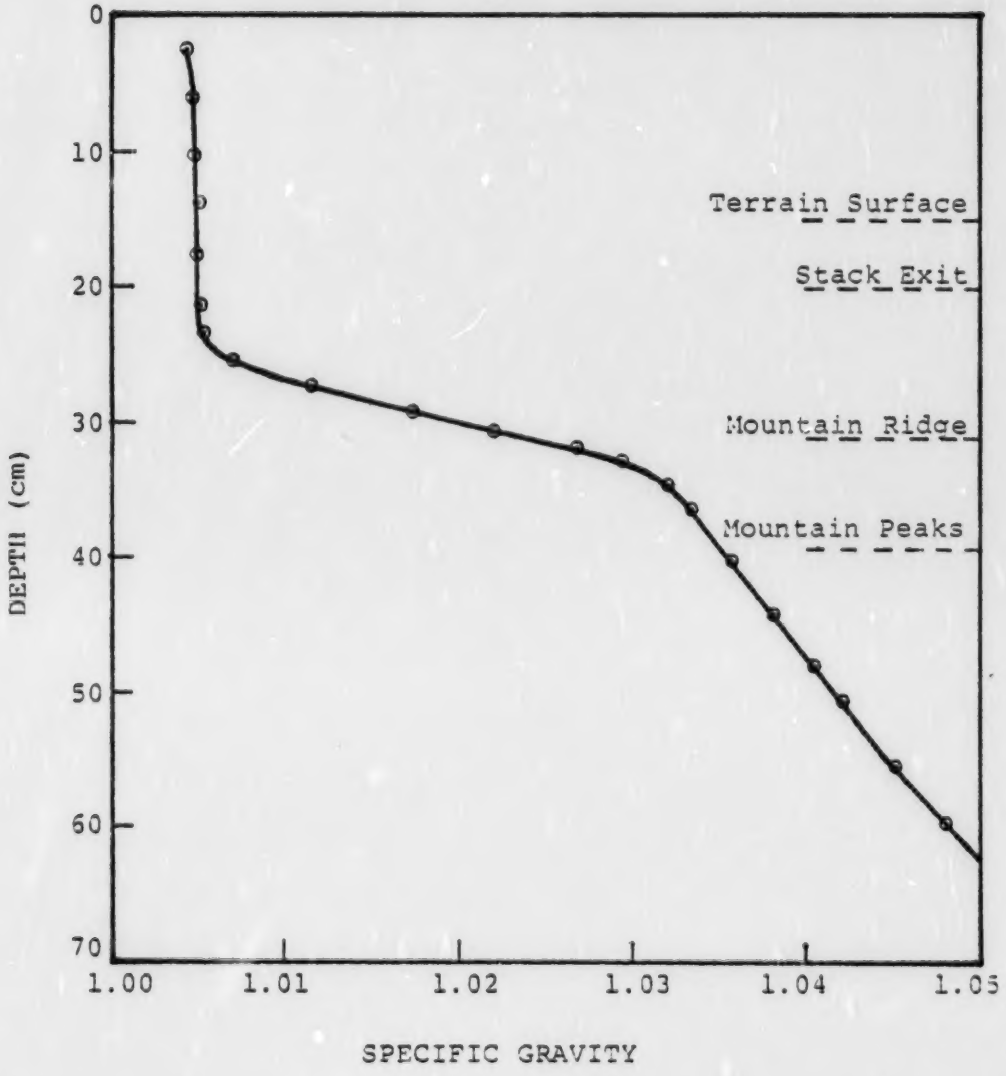

Fig. 5 A Typical 3-Layer Stratification Profile Measured With a Conductivity Probe in the Towing Tank (Runs IIa and IIb)

SECTION V

PLUME DISPERSION IN 3-LAYER STRATIFIED FLOWS

For the experiments, a 3-layer stratified fluid was prepared in the towing tank to simulate an elevated inversion layer in the atmosphere. Figure 6 shows two sketches of the structure of the 3-layer fluid. Figure 5 corresponds to the actual density profile of fig. 6b (upside down model). The 3-layer fluid consists of a neutral layer (constant density) adjacent to the ground, a neutral (fig. 6a) or a stable (fig. 6b) layer high above the ground layer, and an extremely stable or inversion layer between the two. Figure 6 also shows the reference elevations of the idealized terrain model and of the stack. We purposely arranged the top of the middle inversion layer at a level above the mountain ridge so the plume would not rise above the mountain.

In the experiment, we conducted two (2) runs for each of the two 3-layer stratified cases (fig. 6). Table 2 lists the experimental conditions for all four (4) runs. The free-stream wind speed is denoted by U_∞, and the ratio of the effluent speed W_s to U_∞ is denoted by K. The stack Froude number, F_D, is defined as $F_D = W_s/\sqrt{gD\Delta\rho/\rho_s}$, where D is the stack diameter, $\Delta\rho$ is the difference in the densities of the effluent and the ambient fluids at the stack exit, g is the gravitational acceleration and ρ_s is the effluent density. The internal Froude number, F_{hi}, is defined as $F_{hi} = U_\infty/N_i h$, where $F_{hi} = U_\infty/N_i h$, N_i is the Brunt-Vaisala frequency of the i^{th} layer, and h is the height of the mountain ridge.

5.1 Flow Visualization

Figure 7 shows the side and plan views of the plumes in 3-layer stratified flows over the idealized terrain model. The side views (figs. 7a through 7d) indicate that the overall dispersion patterns resemble, to some degree, those observed in 1-layer stratified flows (figs. 15 through 18 in [I]), especially in the region upstream of the mountain.

In the near field, the turbulent motion in the plume dominates the plume dispersion. The plumes released into the bottom neutral layer rise into the middle inversion layer. Overshooting of the plumes, in the inversion layer for the low internal Froude number (figs. 7a and 7c) is evident.

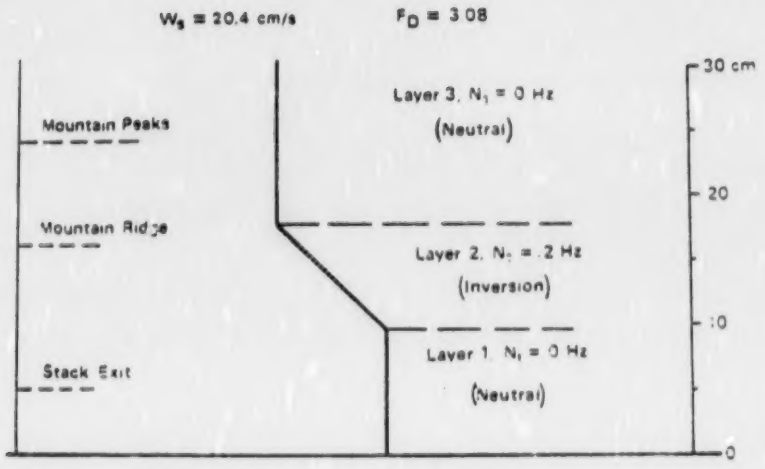

a. Runs Ia and Ib

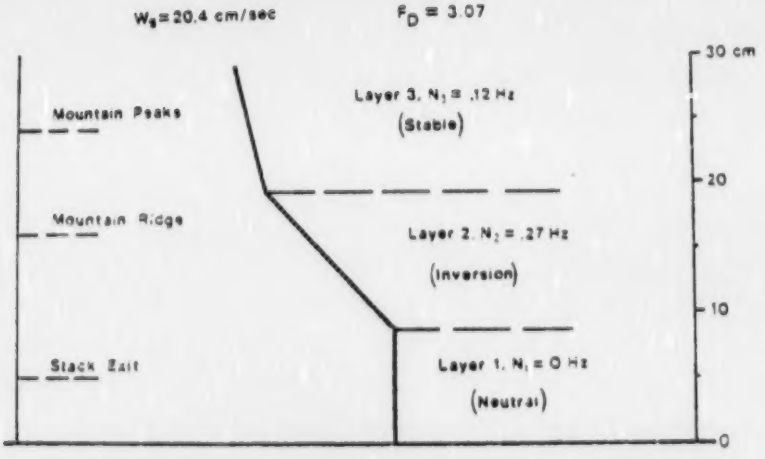

b. Runs IIa and IIb

Fig. 6 3-Layer Stratification Structure for the Simulation of Plume Dispersion Into an Elevated Inversion Layer

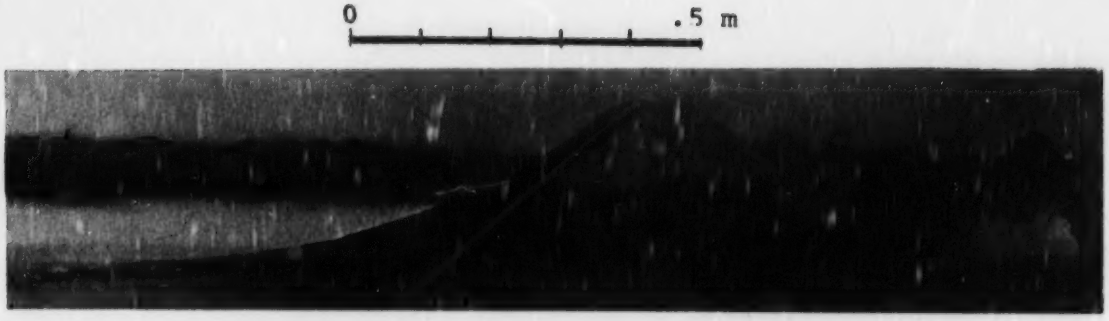

a. Run Ia, U_∞ = 3 cm/s, K = 6.8, F_{h2} = .92

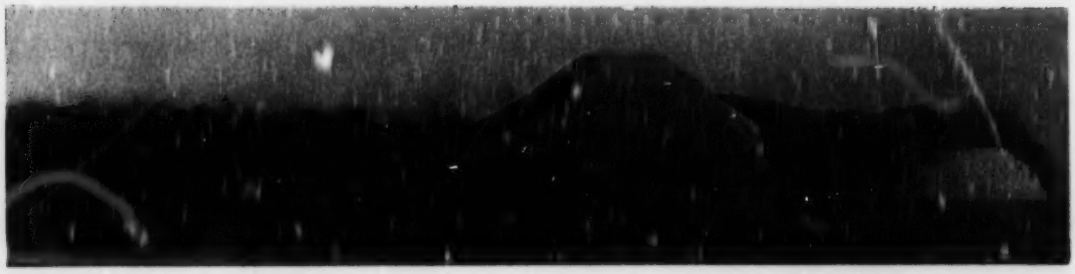

b. Run Ib, U_∞ = 6 cm/s, K = 3.4, F_{h2} = 1.85

c. Run IIa, U_∞ = 3 cm/s, K = 6.8, F_{h2} = .68

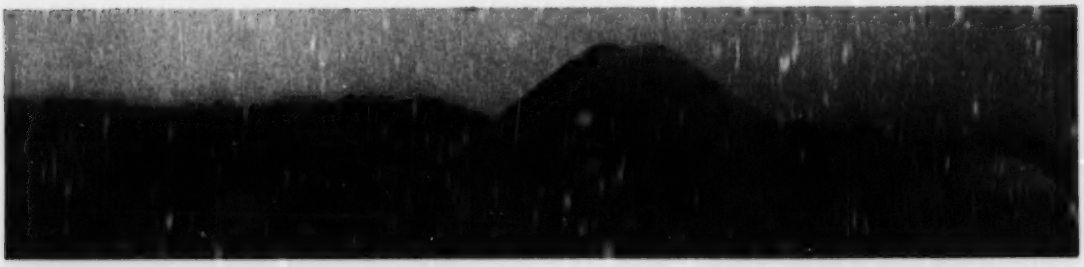

d. Run IIb, U_∞ = 6 cm/s, K = 3.4, F_{h2} = 1.37

Fig. 7 Plume Dispersion Into an Elevated Inversion Layer Over the Idealized Terrain Model. F_D = 3.08

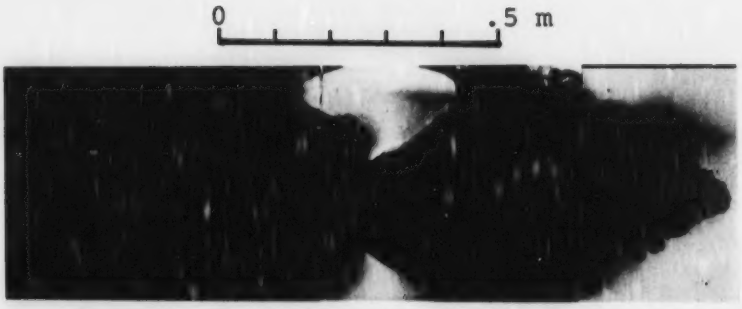

e. Run Ia, U_∞ = 3 cm/s, K = 6.8, F_{h2} = .92

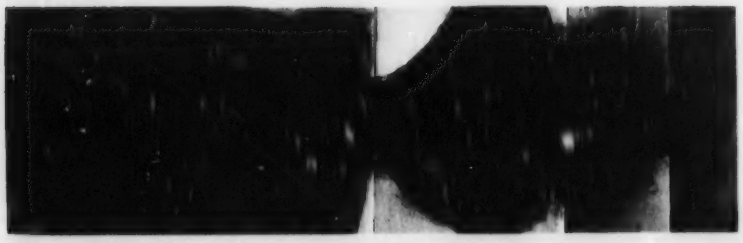

f. Run Ib, U_∞ = 6 cm/s, K = 3.4, F_{h2} = 1.85

g. Run IIa, U_∞ = 3 cm/s, K = 6.8, F_{h2} = .68

h. Run IIb, U_∞ = 6 cm/s, K = 3.4, F_{h2} = 1.37

Fig. 7 (Cont'd) Plume Dispersion Into an Elevated Inversion Layer Over the Idealized Terrain Model. F_D = 3.08

The bent-over plumes level off and are trapped within the inversion layer. The vertical spreads of the leveling plumes increase with an increase in internal Froude number, F_{h2}. Compared with the corresponding cases in [I], the vertical and lateral spreads of all the present cases are quite large as a result of the relatively large spreading rate in the bottom neutral layer.

Farther downstream, the mountain blocks the flows in the inversion layers. For all the cases, the pollutants in the plumes are carried by the wind, at least partially, around the mountain. Direct impingement of the plume onto the mountain slope is evident. For the low internal-Froude-number cases (figs. 7a and 7c), the plumes are aloft upstream and downstream of the mountain. The wind carries the pollutants around the mountain at the same level as those upstream and downstream of the mountain. This phenomenon implies that the vertical displacements of the streamlines around the mountain are small. When the internal Froude numbers are doubled (figs. 7b and 7d), the wind forces the pollutants carried around the mountains downward to the ground. This complicated dispersion pattern apparently results from the interaction of the stratified flow with the terrain and from the vertical pressure gradient developed as the fluid flows around the mountain slope (see Task II report). Downstream of the mountain, the pollutants which were once aloft at small Froude numbers, are stirred intensively until they reach the ground. As a result, we expect high concentrations on the ground. The tops of the pollutant layer do not show significant differences in the elevation upstream and downstream of the mountain, as opposed to the cases observed in figs. 16 and 18 in [I]. In the present experiment, lee waves cannot penetrate into the bottom neutral layer; and, therefore, the strength of the downslope wind (the descending portion of a lee wave) which tends to carry the pollutants toward the ground, decreases considerably.

Figures 7e through 7h show the plan views of the plumes. The plumes released from the stacks (right) were advected toward the mountain. The I-shaped, white portion shown in fig. 7h corresponds to the peaks and the ridge between the peaks (see, also, fig. 1). For all cases, the plan views (figs. 7e through 7h) show that the wind carries the plumes, at least partially, around the mountain. For the cases with a less stable inversion layer (figs.

7e and 7f), the plumes are carried over and around the mountain while, for the cases with a more stable inversion layer (figs. 7g and 7h), the plumes are carried mainly around the mountain. This result demonstrates that the plume rise decreases while the upstream blocking increases with increasing stability. Comparing the individual cases with the same stratification profile, we find the initial lateral spread decreases while the plume rise increases with an increasing internal Froude number, F_{h2} (fig. 7e vs. 7f and 7g vs. 7h).

The two cases with a more stable, middle inversion layer (figs. 7g and 7h) are strikingly different. For the low internal-Froude-number case, the valley just downstream of the mountain ridge is practically free of pollutants (fig. 7g). The pollutants, which are carried by the wind around the mountain, are transported downstream along the outside contour of the mountain. On the other hand, for the high internal-Froude-number case (fig. 7h), the valley is filled with pollutants. In this case, a strong reverse flow, which carries pollutants from the sides into the valley, appears to develop in the lee of the mountain. A small portion of the pollutants trapped in the downstream valley is contributable to those carried over the mountain ridge (see, also, the movie).

5.2 The Velocity Profile

Hot-film probes on the x-z plane at the stack location measured the mean velocity profile, $\overline{U}(z)$, of Run IIb. Figure 8 shows these measurements. A dotted line in fig. 8 denotes the free-stream wind or towing speed, U_∞. The profile shows several interesting features, which are the consequences of the interaction between the stratified flow and the topography. The wind speed in the middle inversion layer, where the flow is blocked by the mountain ridge (upstream blocking), appears to be at a minimum. In the bottom neutral layer, the velocity is higher than that in the middle layer because upstream blocking does not occur in a neutrally stable flow. In the upper stable layer, where no major obstacle blocks the flow, we measured strong overshooting from the mean wind or towing speed. Overshooting is an established characteristic of stably stratified flows (Long, 1959 and Pao, 1968). The profile displays several regions of high vertical shear. The most pronounced shear region occurs just above the mountain ridge, between

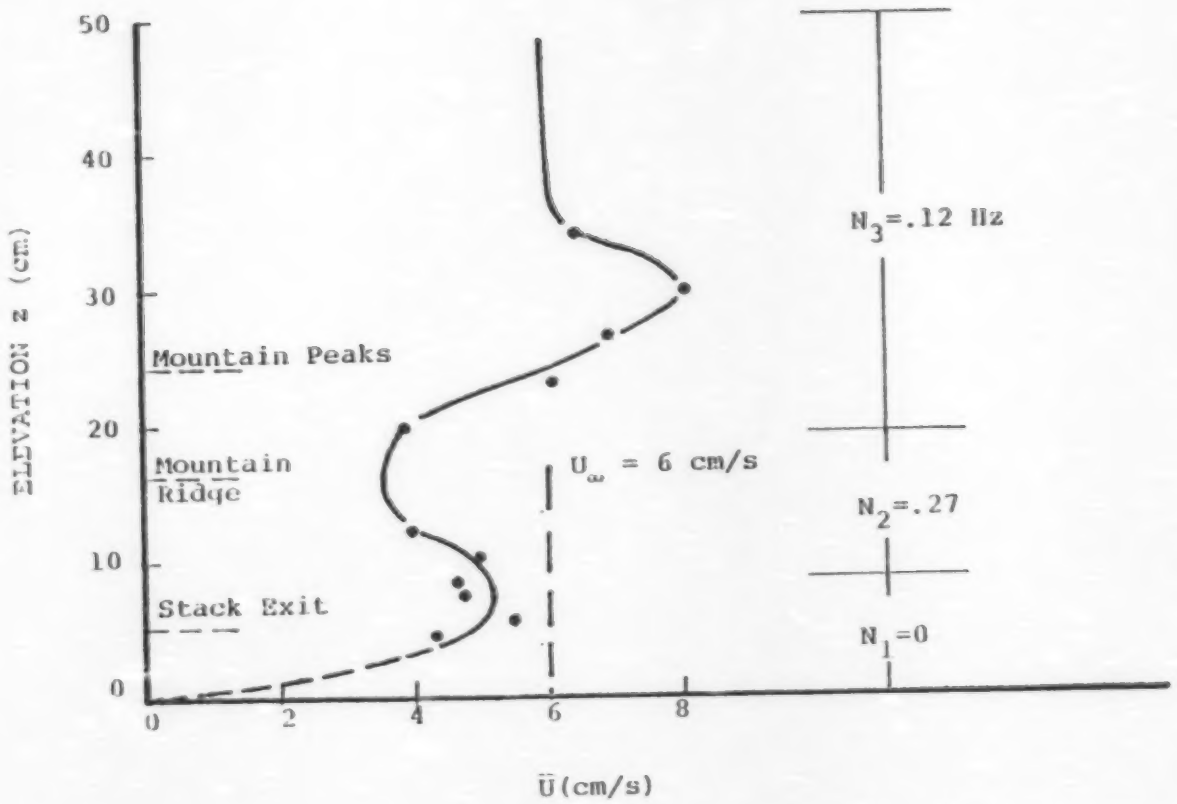

Fig. 8 Mean Velocity Profile at the Location of the Stack in Run IIb. The Ambient Fluid Was Stratified With a 3-Layer Structure. The Idealized Terrain Model Was That Described in Section 5.9

the blocked and the overshooting regions. The visualization results (fig. 7) show that the plume levels off at an elevation slightly below that of the mountain ridge, where the flow is noticeably blocked.

5.3 Concentration Measurements

Ten (10) thermistor probes that were installed in the terrain model measured the ground concentration on the mountain slope. Their positions are indicated on the contour map shown in fig. 1. Table 3 summarizes the results of Runs Ia, Ib, IIa and IIb.

For Run Ia where F_{h2} = .92, the wind carries the plume over and around the mountain, and maximum ground concentrations occur on the top of the mountain ridge between the peaks (probes nos. 1 and 3) and have values as high as 4,400 ppm relative to the effluent concentration. High ground concentrations were also present at other locations on the mountain slope (probes nos. 4, 5, 9 and 10) at the level where a portion of the pollutants in the plume are carried around the mountain. These measurements further support the observation (Lin, et al., 1974) that direct impingement of a plume onto a mountain slope occurs under stable conditions. The maximum root-mean-square concentration occurred on the mountain ridge (probe no. 3). This location corresponds to that of the plume edge, where the concentration signal is highly intermittent.

When the internal Froude number increases (Run Ib, F_{h2} = 1.85), the plume rise tends to increase slightly, and the ground concentrations on the mountain ridge decrease considerably. The measurement of the highest concentration still occurred at probe no. 1.

In Run IIa, the wind carries the pollutants around the mountain (fig. 7a), and ground concentrations on the ridge are low. The vertical spread is so limited that the plume is not in direct contact with any of the probes. When the internal Froude number increases (Run IIb, F_{h2} = 1.37), the plume rise increases, and a small portion of the pollutants are carried over the mountain ridge. As a result, measurement of concentrations on the ridge were slightly higher (probe no. 1). The vertical spread also increases and high concentrations were measured at other locations on the mountain slope (probes nos. 2, 4, 7 and 10).

Table 3. Ground Concentrations Data of the Sharp Inversion Experiments

Thermistor Probe No.	x [cm]	y [cm]	z [cm]	Run Number					
				Ia			Ib		
				$\bar{\theta}$ [°C]	$(\bar{\theta}-\bar{\theta}_a)/(\bar{\theta}_s-\bar{\theta}_a)$	$\sqrt{\overline{\theta^2}}$ [°C]	$\bar{\theta}$ [°C]	$(\bar{\theta}-\bar{\theta}_a)/(\bar{\theta}_s-\bar{\theta}_a)$	$\sqrt{\overline{\theta^2}}$ [°C]
1	61.00	0.00	16.26	20.75	5.74×10^{-3}	3.82×10^{-2}	20.56	4.02×10^{-3}	2.71×10^{-2}
2	57.47	0.00	8.89	20.37	2.87×10^{-4}	1.36×10^{-3}	20.42	2.01×10^{-3}	2.32×10^{-2}
3	61.00	6.35	16.50	20.62	3.87×10^{-3}	1.04×10^{-1}	20.36	1.15×10^{-3}	4.72×10^{-2}
4	57.47	6.35	11.68	20.44	1.29×10^{-3}	4.44×10^{-2}	20.45	2.44×10^{-3}	5.04×10^{-2}
5	67.00	0.00	12.95	20.65	4.31×10^{-3}	1.39×10^{-2}	20.44	2.29×10^{-3}	3.69×10^{-2}
6	64.77	0.00	14.48	20.37	2.87×10^{-4}	5.89×10^{-3}	20.41	1.86×10^{-3}	3.62×10^{-4}
7	36.83	19.69	10.29	20.35	0.0	1.07×10^{-2}	20.28	0.0	1.12×10^{-2}
8	38.74	19.69	12.09	20.37	2.87×10^{-4}	2.82×10^{-2}	20.33	7.17×10^{-4}	4.83×10^{-2}
9	44.45	19.69	14.10	20.48	1.87×10^{-3}	8.06×10^{-2}	20.38	1.43×10^{-4}	5.21×10^{-2}
10	57.47	13.97	13.97	20.42	1.01×10^{-3}	2.31×10^{-2}	20.32	5.74×10^{-4}	1.69×10^{-2}
Ambient Conditions				20.35	-	1.0×10^{-3}	20.28	-	3.0×10^{-4}

Effluent Temperature $\theta_s = 90 \pm 2^{\circ}C$

Table 3. (Cont'd) Ground Concentrations Data of the Sharp Inversion Experiments

Thermistor Probe No.	x [cm]	y [cm]	z [cm]	Run Number					
				IIa			IIb		
				$\bar{\theta}$ [°C]	$(\bar{\theta}-\bar{\theta}_a)/(\bar{\theta}_s-\bar{\theta}_a)$	$\sqrt{\overline{\theta^2}}$ [°C]	$\bar{\theta}$ [°C]	$(\bar{\theta}-\bar{\theta}_a)/(\bar{\theta}_s-\bar{\theta}_a)$	$\sqrt{\overline{\theta^2}}$ [°C]
1	61.00	0.00	16.26	19.93	4.28×10^{-4}	2.65×10^{-3}	20.00	1.43×10^{-3}	7.46×10^{-2}
2	57.47	0.00	8.89	19.91	1.43×10^{-4}	1.70×10^{-3}	20.12	3.14×10^{-3}	5.12×10^{-2}
3	61.00	6.35	16.50	19.92	2.85×10^{-4}	4.42×10^{-3}	19.95	7.13×10^{-3}	8.92×10^{-3}
4	57.47	6.35	11.68	19.90	0.0	4.30×10^{-3}	20.29	5.56×10^{-3}	6.93×10^{-3}
5	67.00	0.00	12.95	19.91	1.43×10^{-4}	2.02×10^{-3}	19.96	8.56×10^{-4}	3.51×10^{-2}
6	64.77	0.00	14.48	19.92	2.85×10^{-4}	1.01×10^{-3}	19.93	4.28×10^{-4}	2.32×10^{-3}
7	36.83	19.69	10.29	19.91	1.43×10^{-4}	3.82×10^{-3}	20.20	4.28×10^{-3}	1.17×10^{-1}
8	38.74	19.69	12.09	19.91	1.43×10^{-4}	2.13×10^{-3}	19.93	4.28×10^{-4}	9.42×10^{-3}
9	44.45	19.69	14.10	19.92	2.85×10^{-5}	4.80×10^{-3}	19.92	3.14×10^{-4}	6.36×10^{-3}
10	57.47	13.97	13.97	20.01	1.57×10^{-3}	5.57×10^{-3}	20.05	2.14×10^{-3}	2.14×10^{-2}
Ambient Conditions				19.90	-	1.0×10^{-3}	19.90	-	1.0×10^{-3}

Effluent Temperature $\bar{\theta}_s = 90 \pm 2^{\circ}C$

SECTION VI

PLUME DISPERSION FROM THE KENNECOTT SMELTER STACK

To simulate plume dispersion in 1-layer stratified flows over a realistic terrain, we selected one of the stacks at the Kennecott Copper Smelter in Garfield, Utah and the surrounding terrain. Table 4 summarizes the simulation conditions for both the prototype and the model.

The terrain model, whose features are more rugged and asymmetric than the idealized model, had a scale of 1/10,000. To ensure a turbulent plume, we enlarged the stack diameter by a factor of two (1/5,000 scale). According to the discussion in appendix B, the effect of the diameter exaggeration on plume dispersion in the far field is insignificant under given neutral or stable conditions, as long as the buoyancy number in the model remains the same as that in the prototype. The buoyancy number in the exaggerated stack was preserved by reduction of the speed ratio, K, by 21% (see appendix B).

6.1 Flow Visualization

Figure 9 show plumes in stably stratified flows (1-layer) over the rugged terrain model southeast of the Kennecott Copper Smelter in Garfield, Utah. The plumes in both cases (Run IIIa and IIIb), with F_h = 1.04 and 2.08, respectively, are quite close to the ground. The vertical and lateral spreads of the plumes, although quite different in the two cases, are small compared to the vertical and horizontal extents of the area modeled.

For the low internal-Froude-number case (fig. 9a), where F_h = 1.04, the overall shape of the plume conforms closely to the underlying terrain features. The plume is aloft over the entire length of the model. Far downstream of the stack, the plume tends to relaminarize. This relaminarization indicates that the turbulence intensity at the plume level, although quite close to the ground, is low and the turbulent boundary layer (TBL) is very thin.

When the internal Froude number increases by a factor of two (fig. 9c) and F_h = 2.08, the overall shape of the plume tends to smoothen out. The vertical and lateral spreads increase considerably, and the wind carries the pollutants in the plume downward to the ground. No tendency of relaminarization

Table 4. Simulation Conditions for Plume Dispersion From the Kennecott Copper Smelter Stack

a. Characteristic Length

Length Scale: 1/10,000

Description	Prototype [m]	Model [cm]
Stack Diameter, D	8.23	.17*
Stack Height, H	124	12.4
Elevation of Coon Peak	2,760	27.6
Characteristic Height, h	1,480	14.8

*Enlarged by a factor of two

b. Simulation Conditions

Description	Prototype		Model	
	Run IIIa	Run IIIb	Run IIIa	Run IIIb
Free-Stream Wind Speed, U_∞ [m/s]	6.1	12.2	.02	.04
Effluent Speed, Ws [m/s]	15.24	15.24	.04	.04
Brunt-Vaisala Frequency, N [Hz]	.004	.004	.13	.13
Internal Froude Number, F_h	1.04	2.08	1.04	2.08
Speed Ratio, K	2.5	1.25	2.0	1.0
Stack Froude Number, F_D	2.11	2.11	2.02	2.02
Lapse Rate, $-\frac{\partial\theta}{\partial z}$ [°C/100m]	.78	.78	--	--
Ambient Temperature, $\bar{\theta}_a$ [°C]	0	0	20.6	20.6
Effluent Temperature, θ_s [°C]	177	177	90	90
Effluent Density, ρ_s [gm/cm^3]	--	--	1.035	1.035

a. Run IIIa, Side View, U_∞ = 2 cm/s, K = 2.0, F_h = 1.04

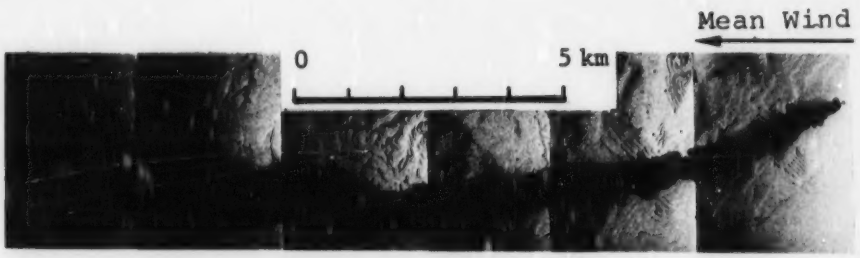

b. Run IIIa, Plan View, U_∞ = 2 cm/s, K = 2.0, F_h = 1.04

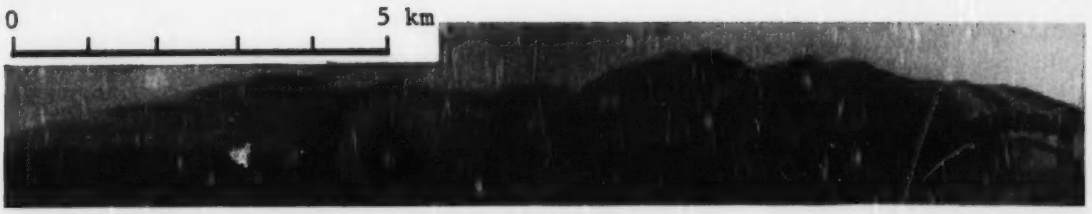

c. Run IIIb, Side View, U_∞ = 4 cm/s, K = 1.0, F_h = 2.08

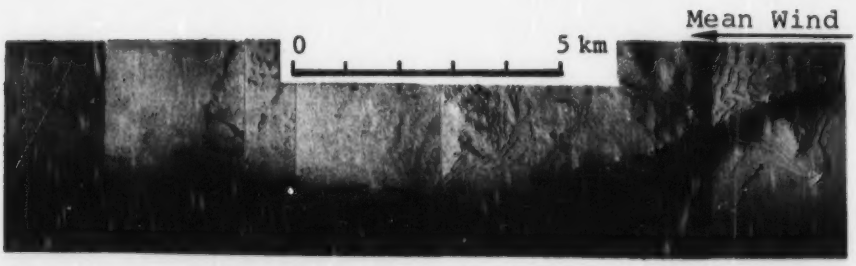

d. Run IIIc, Plan View, U_∞ = 4 cm/s, K = 1.0, F_h = 2.08

Fig. 9 Dye Visualization of Plume Dispersion From a Stack Located at the Kennecott Copper Smelter in Garfield, Utah, Under Stable Conditions. Wind Direction = 315°. F_D = 2.02

of the plume is observable, and the plume edges are relatively ill-defined. This phenomenon indicates that the thickness of the TBL has increased to include the plume and that the turbulence intensity at the plume level increases.

The importance of terrain effects on plume dispersion in stably stratified flows are unambiguously demonstrated by the plan views of the plumes (figs. 9b and 9d). The wind definitely carries the plumes around Oquirrh Mountain and diverts it into Little Valley, which is northeast of the mountain. In the near field, the terrain effects are so dominant that the initial diversion ($\sim 20^{\circ}$ from the free-stream wind direction) of the plume is independent of the internal Froude number. For both cases, the plumes are carried into Little Valley avoiding the steep mountain slope on the southwest of Oquirrh Mountain. For the low internal-Froude-number flow, $F_h = 1.04$, the wind seems to carry the plume into the valley along the foothill of Oquirrh Mountain. Farther downstream, in the lee of the mountain, the plume tends to turn back to follow the mean wind. When the internal Froude number is double, the plume is carried slightly farther away from the mountain toward the northeast.

In the near field, the lateral plume spread of the high internal-Froude-number case is slightly smaller than that of the low internal-Froude-number case. This reduction is present because the turbulent motion in the plume dominates the plume dispersion. In the experiment, we increased the internal Froude number for the same stratification by increasing the towing speed. The plume in the low internal-Froude-number case, therefore, has a relatively long time to spread before the wind advects it to a fixed downstream location. As the plume is advected farther downstream, however, the role of the background turbulence becomes increasingly important. In the far field, the lateral plume spread in the high internal-Froude-number case becomes considerably larger than that in the low internal-Froude-number case because the turbulence intensity at the plume level is higher in the former than that in the latter.

Under neutral conditions, a plume rises considerably higher with a larger vertical spread and a much smaller lateral diversion than under stable conditions (Veenhuizen, et al., 1973). These distinctive differences are not surprising because the vertical motion in a neutral flow is not inhibited

and because the buoyant plume tends to rise above rather than around the mountain. The large lateral diversion observed in the stable cases is the result of upstream blocking, which does not occur in the neutral cases. The generation and maintenance of a thick TBL with high turbulence intensity further disperses the plume as the neutral fluid flows over the rugged terrain.

6.2 Probe Measurements

6.2.1 Velocity Profiles

Figure 10 shows the mean velocity profiles, $\overline{U}(z)$, of Runs IIIa and IIIb, which we measured with hot-film probes at the stack location. The dotted lines denote the free-stream speed for the respective runs. Both profiles show blocked regions at low levels and overshooting regions high above the blocked regions. The abnormally large overshooting from the mean wind speed is the result of blocking induced by the tall and massive mountain ridge on the southwest of the smelter. This ridge includes Kessler Peak (elev. 2689 m) and Coon Peak (elev. 2760 m) of Oquirrh Mountain. From the visualization results, the plumes were released in and appear to remain in the blocked regions.

6.2.2 Concentration Measurements

Based on the visualization results, locations were selected to install ten (10) thermistor probes for the measurement of ground concentrations (see fig. 2). The probes were installed to cover an area large enough that the distribution of ground concentrations could be inferred from the data. The background concentrations were measured with probes installed outside the plumes.

For both Runs IIIa and IIIb, the results show no appreciable ground concentrations at any of the locations inside and outside the plumes. The measured temperatures were all comparable with the thermal noise level ($.01^{\circ}C$) in the towing tank. If a source SO_2 concentration of 2000 ppm is assumed, the noise level of $.01^{\circ}C$ is equivalent to a full-scale noise level of .28 ppm, which is lower than the Federal Secondary Ambient Air Quality Standard of .5 ppm (3-hr average). In the experiment, the sampling time was about 60 seconds, which is equivalent to a sampling time of 1/2 hour in the full-scale case (time scale = 1/33). Note that the experiment was designed to simulate a steady wind condition.

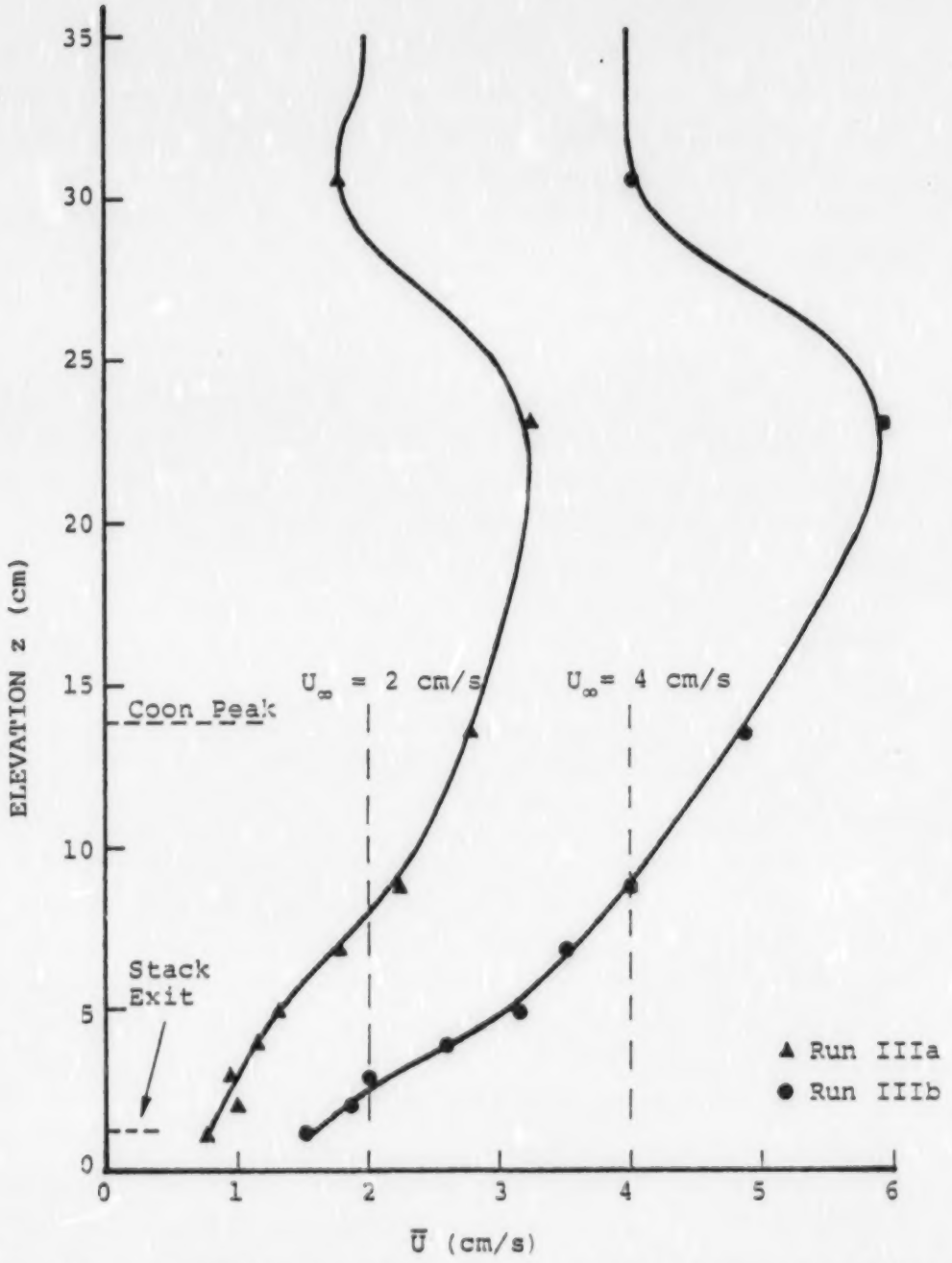

Fig. 10 Mean Velocity Profiles at the Location of the Stack in the Kennecott Smelter Model. Wind Direction = 315°.

From the visualization results, we expect the ground concentrations in Run IIIa to be low because the plume is aloft throughout the entire length of the model. In Run IIIb, however, pollutants in the plume appear to be stirred and carried to the ground. Apparently, the turbulent motion enhances the plume spread, and the pollutants have been diluted greatly.

SECTION VII

PLUME DISPERSION DURING INVERSION BREAKUP

After a nocturnal inversion is formed, a plume released into the stable layer is transported downwind in the form of a flat ribbon with variable lateral spreading and minimum vertical dispersion. Subsequently, as the result of surface heating, a growing unstable layer below replaces the nocturnal inversion. As the thermally induced vertical mixing develops and builds to include the plume, pollutants in the plume are entrained into the unstable layer and are uniformly stirred and carried to the ground. Thomas, et al. (1970) measured maximum ground concentrations in a narrow band along the plume axis during the inversion breakup period. The unsteady, convective motion, also termed penetrative convection, has been the subject of some full-scale study (Lenschow and Johnson, 1968 and Thomas, et al., 1970) and of some theoretical modeling (Lilly, 1968). In the laboratory, Deardorff, et al. (1969) investigated the penetrative convection in a tank filled with thermally stratified distilled water. Subsequently, Willis and Deardorff (1974) conducted experiments to study the rate of dispersion of nonbuoyant particulates released from a near-ground source into the convective layer.

In this study, we attempted to develop a method of simulating the penetrative convection in the atmosphere by releasing either heat or mass from a surface to initiate and to maintain the growth of the unstable layer adjacent to the ground. Pollutants are released from a stack to allow investigation of the dispersion characteristics during the unsteady inversion-breakup period. For realistic simulation of the unsteady inversion-breakup phenomena, several conditions, in addition to those described in $[I]$, must be satisfied. Geometric similarity requires that the maximum height of the unstable layer, z_i, be simulated correctly, i.e.,

$$\frac{[z_i]_m}{[z_i]_p} = \frac{[D]_m}{[D]_p} \quad , \tag{7.1}$$

where the subscripts m and p refer to the model and the prototype, respectively. Kinematic similarity requires

$$\left[\frac{U_\infty}{w_*}\right]_m = \left[\frac{U_\infty}{w_*}\right]_p \quad , \tag{7.2}$$

where w_* is a convective velocity scale (Deardorff and Willis, 1975). In the present study, however, we made no attempt to satisfy eq. (7.2).

When simulating any unsteady phenomena, one must define the characteristic time scale, T, which is the ratio of the length scale to the velocity scale. Correct simulation of the unsteady inversion-breakup phenomenon requires

$$\frac{\left[T_i\right]_m}{\left[T_i\right]_p} = \frac{\left[T\right]_m}{\left[T\right]_p} \tag{7.3}$$

where T_i is the time required for the unstable layer to reach its maximum height.

We conducted several tests to develop a method to simulate inversion breakup. First, we generated the growth of the unstable layer adjacent to a surface by allowing a heavy salt solution to infiltrate slowly through the surface (an upside-down model). Although we could easily control the penetration height by varying the density of the salt solution, the observed convective motion lacked the large-scale components (the growing "dome" as described by Deardorff, et al., 1969) observed in the field. These large-scale components are responsible for the fumigation of a plume in an unstable layer. Second, we used ice in an attempt to generate the convective motion, but because the heat flux was not sufficiently large (the stable fluid was at a temperature of 20°C), the penetration height was too small to include the plume. Finally, we tested dry ice and obtained satisfactory results.

A special device was designed by FRI to facilitate the experiment. First, we filled two aluminum channels (6.1 m x 7.6 cm x .32 cm) with dry ice and then placed them into the towing tank. The bottom of the channels were in direct contact with the water surface. Between the channels was a gap of 1.3 cm, through which we would tow the stack to simulate plume dispersion in a crosswind.

The field conditions at the TVA Paradise Power Plant on 13 September 1966 (Thomas, et al., 1970) were simulated at FRI in this experiment. Two 183-m stacks are located in the Paradise Plant, but only one of them was in operation on that day. Table 5 lists all the experimental and the

Table 5. Simulation Conditions for the Inversion Breakup Experiments

a. Characteristic Length

Length Scale: 1/5000

Description	Prototype [m] (TVA Paradise Power Plant)	Model [cm]
Stack Diameter, D	7.92	.158
Stack Height, H	183	3.66

b. Simulation Conditions

Description	Prototype (TVA Paradise Power Plant 9/13/1966)	Model
Free-Stream Wind Speed, U_∞ [m/s]	0, 4.88	0, .020
Effluent Speed, Ws [m/s]	18.0	.075
Ambient Temperature, $\overline{\theta}_a$ [°C]	20.6	23.0
Stack Effluent Temperature, θ_s [°C]	144	23.0
Lapse Rate Before Breakup, $-\frac{\partial \overline{\theta}}{\partial z}$ [°C/100m]	-1.2	---
Lapse Rate After Breakup, $-\frac{\partial \overline{\theta}}{\partial z}$ [°C/100m]	.98	---
Brunt-Vaisala Frequency Before Breakup, N [Hz]	.0043	.09
Effluent Density, ρ_s [gm/cm^3]	---	1.043
Ambient Fluid Density, $\overline{\rho}_a$ [gm/cm^3]	---	1.005
Internal Froude Number, F_H	0, 6.20	0, 6.10
Stack Froude Number, F_D	3.15	3.15
Speed Ratio, K	∞, 3.69	∞, 3.76

simulated prototype conditions. Figure 11 shows the actual and idealized profiles of the temperature soundings before and after the inversion breakup. The atmosphere adjacent to the ground was stably stratified and was nearly isothermal at 0658. It finally became neutrally stratified (adiabatic) at 0934. The terrain surrounding the plant site is relatively flat, as shown on the USGS topography map. The terrain effect on the plume released from the 183-m stack under stable conditions will probably be insignificant except very close to the ground. Field observations of the Keystone plume (Schiermeier and Niemeyer, 1968 - figs. 11 and 12), where the terrain features appear to be more rugged than those of the Paradise plant, have substantiated, at least qualitatively, the above statement. For a feasibility study of the simulation of the inversion breakup, representation of the surrounding terrain by a flat surface is therefore sufficient.

7.1 Flow Visualization

To visualize the structure of the growing unstable layer, we used the shadowgraph method described in [I]. Figure 12 is a plot of the penetration height $z_i(t)$. The average of z_i was measured from shadowgraph pictures. The initial slope of the data indicates that z_i is proportional to $t^{1/2}$ before the convection stablizes, which agrees with the observation of Turner (1968). In the present experiment, we cooled the fluid by a constant temperature rather than by a constant heat flux. This cooling process explains the leveling off of the curve at large times, as the temperature in the fluid approaches that of the cooling surface. The time required for z_i to reach its maximum of 10.5 cm (1700 m in the prototype) is about 8 minutes (3 hours in the prototype), which is in the same range as the simulated conditions given in table 5 and fig. 11.

Figure 13 is a series of shadowgraph pictures which show the growth of the unstable layer with time. A plume released into the calm (no cross-wind), stable layer is also shown in each picture.

The interface between the unstable and stable layer is distinctive, but irregular, as shown in fig. 13. Frequently, individual thermals with well-defined boundaries form and rise into the stable layer. The larger the size of the thermal, the higher it rises. Penetration of large thermals into the stable layer occurs frequently and randomly at the interface. The frontal boundaries of these large thermals in the

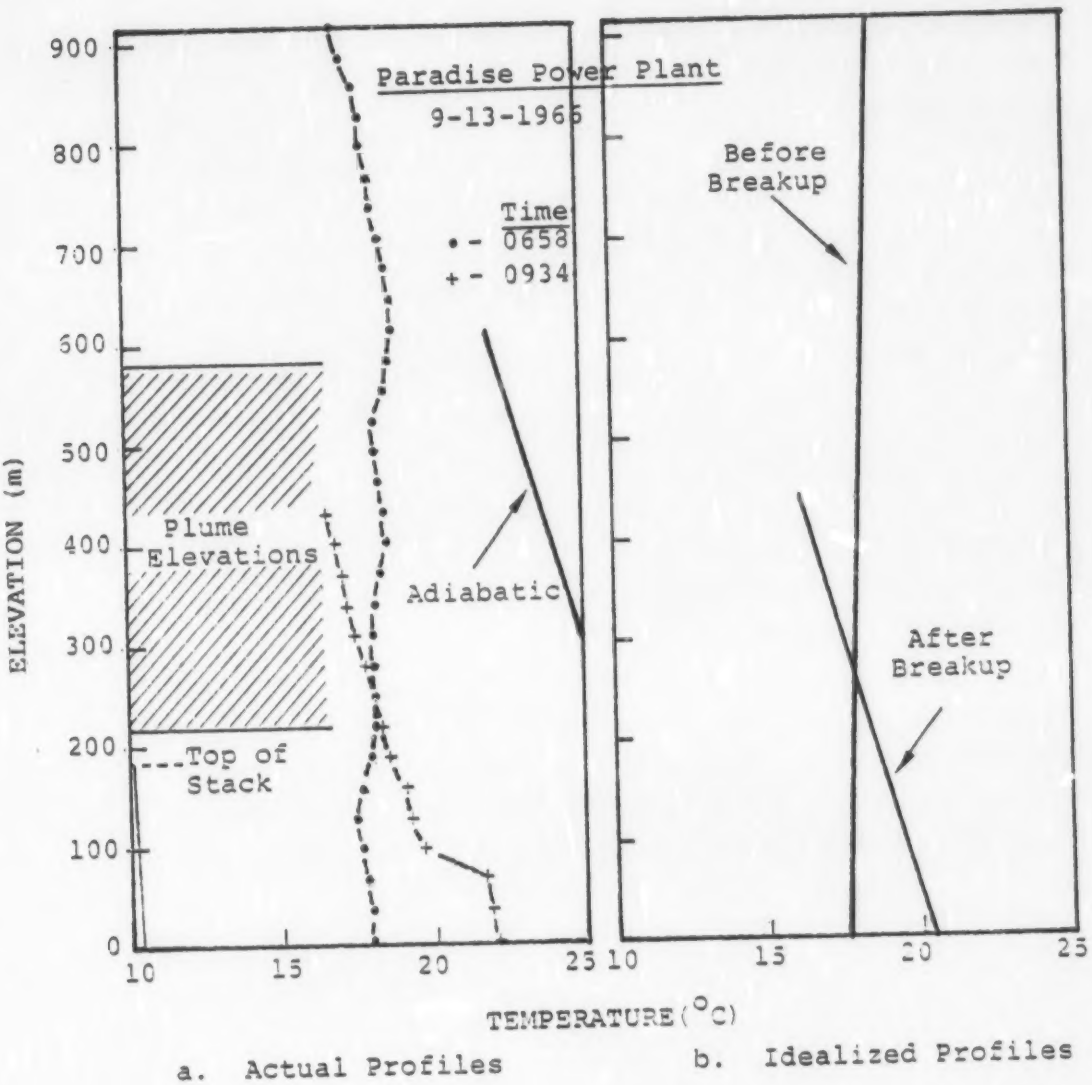

a. Actual Profiles b. Idealized Profiles

Fig. 11 Typical and Idealized Temperature Profiles for the Inversion Breakup Experiment (see Thomas, et al., 1970)

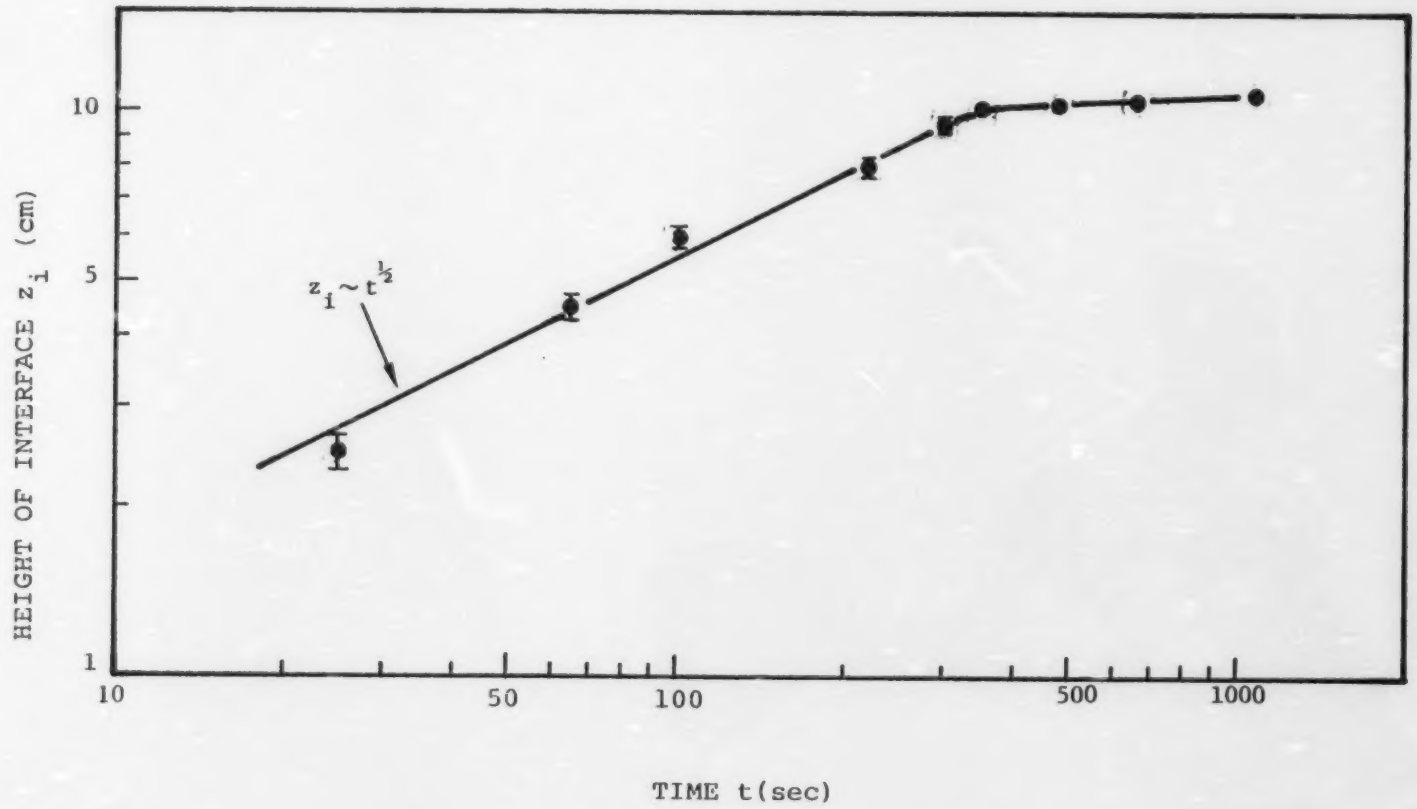

Fig. 12 Penetration Height $z_i(t)$ of an Unstable Layer Generated by Cooling a Surface With Dry Ice in a Stratified Fluid (N ~.1 Hz)

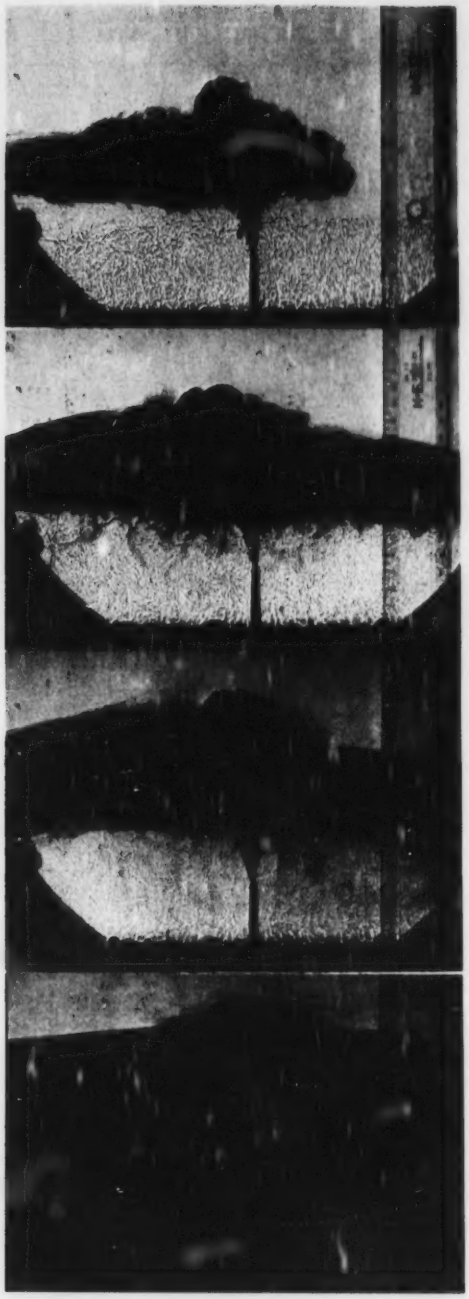

Fig. 13 Shadowgraph Pictures of Entrainment of Pollutants in a Growing Unstable Layer During Inversion Breakup

$U_\infty = 0$, $N = .09$ Hz, $K = \infty$, $F_H = 0$, $F_D = 3.15$

stable layer take the shape of a dome (Deardorff, et al., 1969). Individual domes always overshoot the interface and then subsequently recede. The repetition of the overshooting and receding motions of the large thermals appear to contribute efficiently to the growth of the unstable layer. Between domes, cusp-shaped regions, through which the undisturbed fluid is entrained into the unstable layer, are observed. The intensity and frequency of the generation of large thermals decrease with time. A sharp and relatively smooth interface develops as the penetrative motion becomes less vigorous. The sharp interface observed in the shadowgraph pictures corresponds to the "super" stable region measured by Deardorff, et al. (1969).

When simulating a crosswind, we towed the stack as soon as we secured the channels filled with dry ice. Figure 14 is a series of pictures, in sequence, which show, by tagging the same patch of pollutants in the plume (the camera was stationary to the towing tank), the evolution of the entrainment process. Before the unstable layer builds to reach the plume levels, pollutants in the plume remain aloft. As soon as the top of the growing unstable layer reaches the plume level, pollutants begin to become entrained in the unstable layer (fumigation). As the convective motion continues to penetrate the stable layer, it stirs the entrained pollutants within the unstable layer, and a well-mixed layer adjacent to the ground is finally established.

7.2 Temperature Profile During Inversion Breakup

Ten (10) thermistor probes mounted on a strut measured the temperature profile, $\theta(z,t)$, adjacent to the surface (the bottom of the channels) where the growth of the unstable layer began. The gain of the thermistor gauge was modified to cover a temperature range of 25°C. Figure 11b shows a typical calibration curve of a thermistor probe.

The vertical temperature profiles, $\overline{\theta}(z,t)$, adjacent to the ground are plotted in fig. 15. The temperature profiles tend to stablize in about 10 minutes, which is slightly longer than the time required for z_i to reach its maximum (fig. 12). The initial cooling at $t-t_o = 0$ is the result of radiation which came from the bottom of channels before they were secured in place. Note that a kink on the temperature profile at $z \simeq 3$ cm tends to develop after $t-t_o$ exceeds 600 seconds.

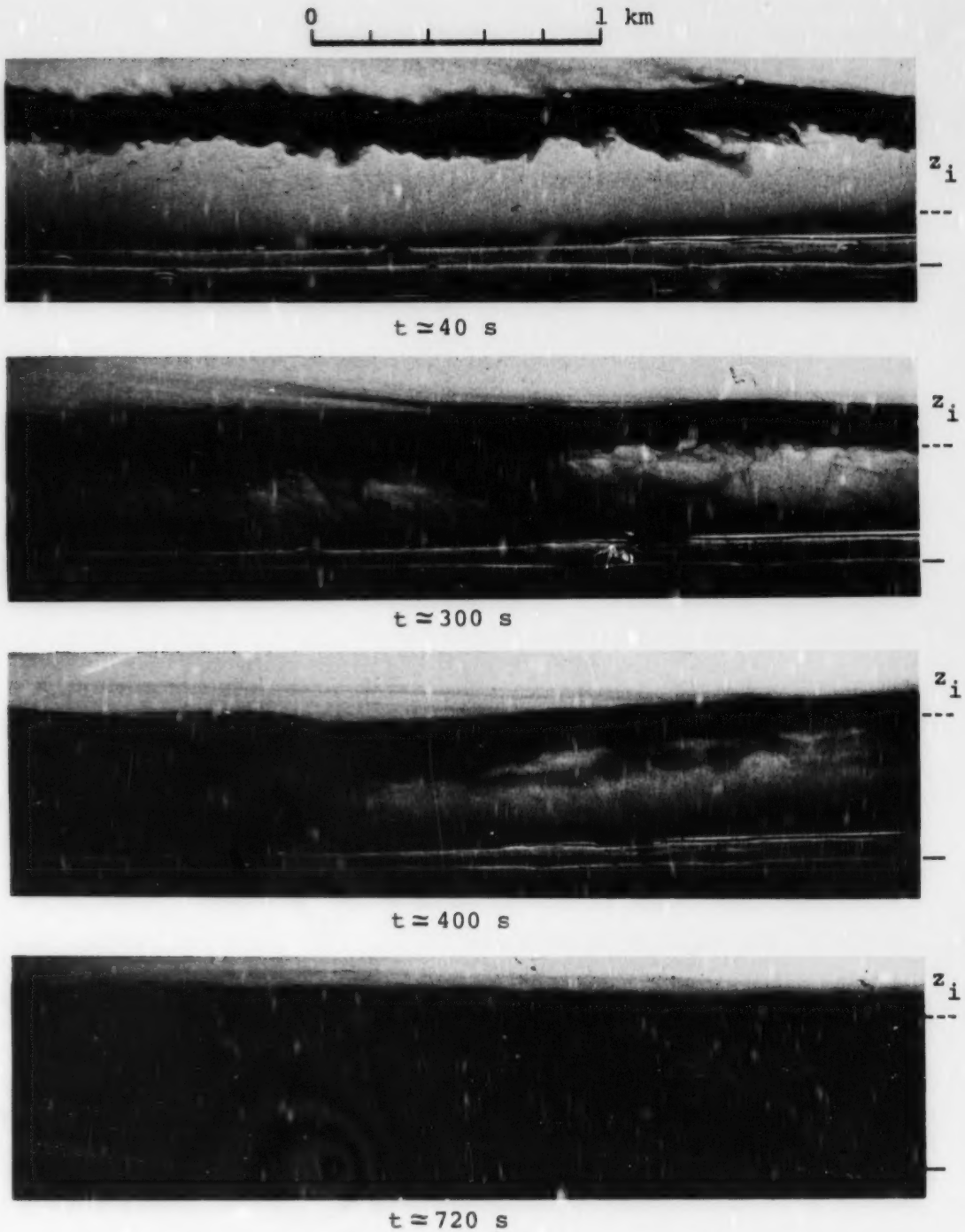

Fig. 14 Dye Visualization of the Sequential Entrainment of Pollutants (Fumigation) in a Growing Unstable Layer During Inversion Breakup. The Pictures Were Taken With the Camera Stationary to the Towing Tank (Following the Same "Patch" of the Plume)

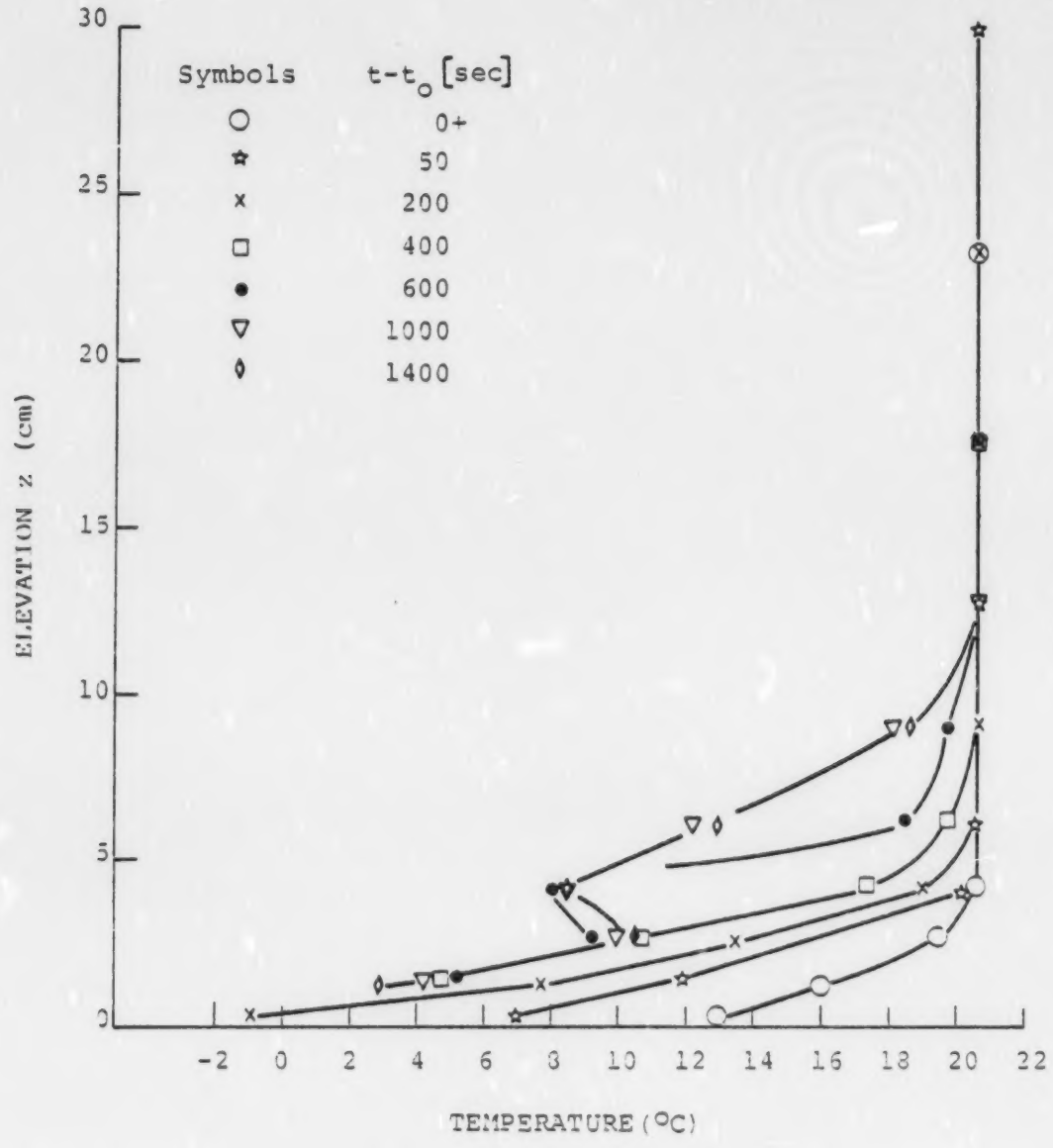

Fig. 15 Temperature Profiles During the Growth of an Unstable Layer Adjacent to a Surface in a Stratified Fluid (N = .095 Hz). The Growth of the Unstable Layer Was Generated by Cooling the Surface With Dry Ice.

REFERENCES

Briggs, G. A. (1969) Plume Rise, U.S. Atomic Energy Commission Critical Review Series, TID-25072.

Deardorff, J. W. and Willis, G. E. (1975) "A Parameterization of Diffusion into the Mixed Layer," Manuscript No. 0201-75-9 (to be published in JAM), National Center for Atmospheric Research, Boulder, Colorado.

Deardorff, J. W., Willis, G. E. and Lilly, D. K. (1969) "Laboratory Investigation of Non-Steady Penetrative Convection," J. Fluid Mech. 35, 7-32.

Defant, A. (1961) Physical Oceanography, vol. 1, Pergamon Press, New York.

Ippen, A. T. (1966) Estuary and Coastline Hydrodynamics, McGraw-Hill, New York.

Lenschow, D. H. and Johnson, W. B. (1968) "Concurrent Airplane and Balloon Measurement of Atmospheric Boundary-Layer Structure Over a Forest," J. Appl. Meteor. 7, 79-89.

Lilly, D. K. (1968) "Models of Cloud-Topped Convection Layer Under a Strong Inversion," Quart. J. R. Meteor. Soc. 94, 292-309.

Lin, J. T., Liu, H. T., Pao, Y. H., Lilly, D. K., Israeli, M. and Orszag, S. A. (1974) "Laboratory and Numerical Simulation of Plume Dispersion in Stably Stratified Flow Over Complex Terrain," Report No. EPA 650/4-74-044, USEPA, Research Triangle Park, North Carolina.

Liu, H. T., Lin, J. T., Pao, Y. H., Veenhuizen, S. D., Peecher, D. W. and Hiatt, G. L. (1974) "The Plume Dispersion in Stably Stratified Flow Over a Flat Plate and a Three-Dimensional Terrain," Flow Research Film No. 6.

Long, R. R. (1959) "The Motion of Fluids With Density Stratification," J. Geophys. Res. 64, 2151-2163.

Martin, S. (1966) "The Slow Motion of a Finite Flat Plate Through a Viscous Stratified Fluid," Tech. Report No. 21 (ONR Series), The Johns Hopkins University.

Pao, Y. H. (1968) "Laminar Flow of a Stably Stratified Fluid Past a Flat Plate," J. Fluid Mech. 34, 795-808.

Pao, Y. H., Lin, J. T., Carlson, R. L. and Smithmeyer, L. P. C. (1971) "The Design and Construction of a Stratified Towing Tank With an Oil-Lubricated Carriage," Flow Research Report No. 4 (APL/JHU POR-3530).

Sanborn, V. A. (1972) Resistance Temperature Transducers, Metrology Press, Fort Collins, Colorado.

Schiermeier, F. A. and Niemeyer, L. E. (1968) "Large Power Plant Effluent Study," (LAPPES), Vol. 1 - Instrumentation, Procedures, and Data Tabulations, National Air Pollution Control Administration Publication No. APTD70-2.

Thomas, F. W., Carpenter, S. B., Leavitt, J. M., Montgomery, T. L., Colbaugh, W. C. (1970) "Report on Full-Scale Study of Inversion Breakup at Large Power Plants," Tennessee Valley Authority, Div. of Environ. Research and Development, Muscle Shoals, Alabama.

Turner, J. S. (1968) "The Behavior of a Stable Salinity Gradient Heated From Below," J. Fluid Mech. 33, 182-200.

Veenhuizen, S. D., Lin, J.-T., Pao, Y.-H., Peecher, D. W. and Hiatt, G. L. (1973) "Laboratory Simulation of Plumes From Kennecott Copper Smelters in Garfield, Utah: Neutral Atmosphere," Flow Research Report No. 9.

Willis, G. E. and Deardorff, J. W. (1974) "A Laboratory Model of the Unstable Planetary Boundary Layer," J. Atmos. Sci. 31, 1297-1307.

Wunsch, C. (1969) "Progressive Internal Waves on Slopes," J. Fluid Mech. 35, 131-144.

APPENDIX A. THE EFFECT OF AN ABSORPTIVE LAYER ON PLUME DISPERSION

In the atmosphere, the upper boundary is nonreflective. Internal waves generated near the ground propagate upward and finally disperse and dissipate into the upper atmosphere. Partial reflection is possible, however, if the outgoing waves encounter sharp inversion layers. In general, we can write the upper boundary condition in the atmosphere as

$$\left.\frac{\partial w}{\partial z}\right|_{z = Z_u} \neq 0, \tag{A.1}$$

where w is the vertical fluid velocity and Z_u is the elevation of the upper boundary considered. In a stratified towing tank, the bottom of the tank imposes a reflective upper boundary condition (since the model is upside down), i.e.,

$$\left.\frac{\partial w}{\partial z}\right|_{z = Z_b} = 0, \tag{A.2}$$

where Z_b is the elevation of the tank bottom in reference to the terrain-model surface.

The reflective boundary condition might cause the formation of unrealistically strong downstream blocking and prevent full penetration of downslope winds toward the leeward surface of the mountain. To resolve this speculation, one could install an absorption layer on the bottom of the towing tank to absorb, at least partially, the internal energy generated by the towed terrain model. We could then observe, with the absorptive layer in place, whether the flow pattern would be more asymmetric and the pollutants would be carried further toward the ground and into the turbulent boundary layer in the lee of the mountain. Absorbers of various types have been applied in the laboratory to reduce reflection of surface and internal waves from tank walls, by Ippen (1966) and Wunsch (1969). The present experiment, however, requires revisions to design an absorptive layer for effectively reducing the reflection of internal waves from the bottom of the towing tank.

Figure 16 shows two plumes in a 1-layer stratified flow over the idealized terrain model. In this experiment, we installed an absorptive layer made with nylon nettings (section 5.1) on the bottom of the towing tank to reduce internal wave reflection. Other experimental conditions were the same as those shown in figs. 17 and 18 in [I]. For the overall dispersion pattern, we observed no significant difference between the corresponding figures, with or without the absorptive layer in place. The direct interaction between the stratified flow and the terrain is so strong, especially close to the terrain surface where plume dispersion is heavily influenced, that the effect of the reflection from the solid bottom becomes insignificant.

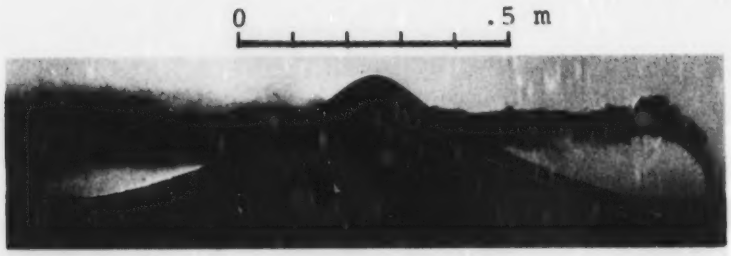

a. Side View, U_∞ = 3 cm/s, K = 6.8, F_h = 1.37

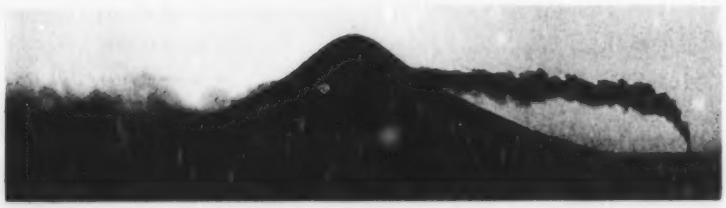

b. Side View, U_∞ = 6 cm/s, K = 3.4, F_h = 2.73

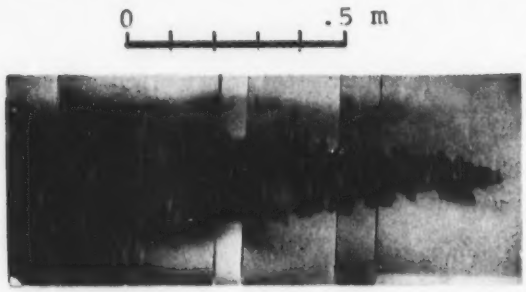

c. Plan View, U_∞ = 6 cm/s, K = 3.4, F_h = 2.73

Fig. 16 Dye Visualization of Plume Dispersion in a Stratified Flow Over the Idealized Terrain Model. An Absorptive Layer Was Installed To Reduce Internal-Wave Reflection. F_D = 3.11. See Figs. 17 and 18 in [I] for Comparison.

APPENDIX B. THE EFFECT OF AN EXAGGERATED STACK ON PLUME DISPERSION

Under neutral conditions, the application of a stack with an exaggerated diameter in simulated plume dispersion has been investigated by Veenhuizen, et al, (1973). The main advantage of this approach is that the flow field is not distorted or disturbed. In the following, we attempt to examine the possible errors involved with the use of an exaggerated stack.

Let a buoyancy number be defined as

$$B = \frac{F}{\bar{U}^3 H} = \left(\frac{K}{F_D}\right)^3 \left(\frac{D}{H}\right)\left(\frac{\rho_s}{4\rho_a}\right), \tag{B.1}$$

where D is the stack diameter, F is the buoyancy flux of the plume, H is the stack height, F_D is the stack Froude number, K is the speed ratio, $\bar{U}$ is the ambient wind speed (assumed to be uniform), and ρ_a and ρ_s are the ambient fluid and effluent density, respectively. By using eq. (B.1), we can rewrite the second equation on p. 33 in Briggs (1969) in a dimensionless form as

$$\left(\frac{Z}{H}\right)^3 = \frac{3B}{2\gamma^2}\cdot\left(\frac{x}{H}\right)^2 + \frac{3}{4}\left(\frac{\rho_s}{\rho_a}\right)K^2\left(\frac{D}{H}\right)\left(\frac{x}{H}\right), \tag{B.2}$$

where Z is the plume trajectory above the stack exit. In the near field when x/H is small, both terms on the right-hand side (r.h.s) of eq. (B.2) are significant. In the far field, where the ratio of the stack diameter to the stack height, D/H is small, we can neglect the second term on the r.h.s of eq. (B.2) except for the very large speed ratio, K. Under neutral conditions, the speed ratio, K, is of order 1. Therefore, if we consider the plume dispersion in the far field, the plume rise depends only on the buoyancy number, B, defined in eq. (B.1).

Under stable conditions, the final height of the tops of plumes Z_t under calm and stable conditions with a constant density gradient is given by Briggs (1969) as

$$Z_t = 5F^{1/4}\, s^{-3/8} . \tag{B.3}$$

Using eq. (B.1) with $s = (2\pi N)^2$, we can rewrite eq. (B.3) as

$$\frac{Z_t}{H} = 1.26B^{1/4}\, F_H^{3/4} . \tag{B.4}$$

Equation (B.3) or (B.5) is also applicable to cases with a light crosswind (Lin, et al., 1974). With the presence of a crosswind, an empirical formula for predicting the final rise of a bent-over plume is also given by Briggs (1969) as

$$Z_c = 4.0\ (F/\bar{U}s)^{1/3} \quad . \tag{B.5}$$

Again, with the use of eq. (B.1), eq. (B.5) can be rewritten as

$$\frac{Z_c}{H} = 1.17B^{1/3}\ F_H^{2/3} \quad . \tag{B.6}$$

Equations (B.2), (B.4) and (B.6) all show that the plume rise in the far field is preserved under a given stable condition, i.e., when F_H is constant, as long as the buoyancy number, B, is identical for the model and the prototype.

Consider plume dispersion experiments which use an exaggerated stack. According to eq. (B.1), there are two ways to preserve the buoyancy number, B. One can reduce the speed ratio ($K \sim L_D^{1/3}$) if F_D remains unchanged, or if K remains unchanged, one can increase the stack Froude number ($F_D \sim L_D^{1/3}$ where L_D is the exaggeration factor of the stack diameter). For example, when we exaggerate the stack diameter by a factor of two, i.e., $L_D = 2$, then we can preserve B, by reducing K by 21% or by increasing F_D by 21%. The optimum choice, however, depends on which regime of the plume we wish to investigate. In the near field, the ratio K is more significant while, in the far field, the stack Froude number is the more important factor.

APPENDIX C. THE RESPONSE OF A HOT-FILM PROBE TO A VARIATION OF FLUID DENSITY

During the calibration of the hot-film probes, the probe strut was lowered about 30 cm to avoid disturbance from the terrain surface. As a result, the probes encountered fluids of different densities during measurement and calibration. In the following, the response of the hot-film probes to the variation of fluid density is examined, and the required correction is evaluated.

Consider an extreme case when a hot-film probe is used to measure the velocity at a level where the fluid density, ρ, = 1.01 and then is calibrated at a different level where $\rho = 1.04$. Neglecting the heat loss to the supports, the rate of production of Joulean heat Q attributable to the current $I = E/R_w$ is equal to the heat loss to the surrounding fluid, that is,

$$E^2/R_w = h\pi D\ell(T_w - T), \tag{C.1}$$

where E is the supply voltage, R_w is the film resistance, h is the heat transfer coefficient, D is the diameter of the cylindrical hot-film probe, ℓ is the length of the sensor, T_w is the film temperature and T is the ambient fluid temperature.

Equation (C.1) can be written to include the Nusselt number $N_u = \frac{hD}{k}$, where k is the thermal conductivity, as

$$E^2 = \pi D\ell R_w(T_w - T)kN_u. \tag{C.2}$$

Note that only k and Nu in the right-hand side of eq. (C.1) depend on the fluid density. After differentiation and normalization, the sensitivity of the hot-film output to density is

$$\frac{\Delta E}{E} = \frac{1}{2}\left(\frac{\Delta k}{k} + \frac{\Delta N_u}{N_u}\right). \tag{C.3}$$

According to King's relation (Sandborn, 1972), we have

$$N_u = .318 + .69\sqrt{Re}, \tag{C.4}$$

where $Re = \frac{UD}{\nu}$ is the Reynolds number. The respective kinematic viscosities for $\rho = 1.01$ and $\rho = 1.04$ are (Martin, 1966)

$$\nu|_{\rho = 1.01} = .00953 \quad \text{and} \quad \nu|_{\rho = 1.04} = .00990 \text{ cm}^2/\text{sec}.$$

For $U = 6$ cm/sec and $D = .002$ in., the Nusselt numbers are

$$Nu|_{\rho = 1.01} = 1.552 \quad \text{and} \quad Nu|_{\rho = 1.04} = 1.529.$$

The thermal conductivity for $\rho = 1.01$ and $\rho = 1.04$ are (Defant, 1961)

$$k|_{\rho = 1.01} = 1.355 \times 10^{-3} \quad \text{and} \quad k|_{\rho = 1.04} = 1.34 \times 10^{-3}$$

(cal/cm sec $^{\circ}$C)

Substituting the above values in eq. (3), we have

$$\left.\frac{\Delta E}{E}\right|_{\Delta\rho = .03} = \frac{1}{2}\{-.023 - .015\}$$

$$= -.02.$$

According to King's law, the velocity-voltage relation is

$$E^2 \sim U^{\frac{1}{4}}. \tag{C.5}$$

Therefore, the corresponding correction for the mean velocity is

$$\frac{\Delta U}{U} \sim 4\left(\frac{\Delta E}{E}\right) \sim -.08. \tag{C.6}$$

As a reference, the experimental error is approximately 10% for mean velocity measurements.

The turbulent velocity is proportional to the local slope of the E-U curve, i.e.,

$$u \sim \frac{dE}{dU}.$$

The correction for u, by using eq. (C.5) and the value of $\left.\frac{\Delta E}{E}\right|_{\Delta\rho = .03}$ is, therefore,

$$\frac{\Delta u}{u} = \frac{\Delta\left(\frac{dE}{dU}\right)}{\left(\frac{dE}{dU}\right)} = -3\left(\frac{\Delta E}{E}\right) = +.06$$

for the extreme case considered.